Unclassified
SECURITY CLASSIFICATION OF THIS PAGE

2

REPORT D

Form Approved
OMB No. 0704-0188

AD-A227 170

1a REPORT SECURITY CLASSIFICATION
Unclassified

1b RESTRICTIVE MARKINGS

2a SECURITY CLASSIFICATION AUTHORITY

3 DISTRIBUTION/AVAILABILITY OF REPORT
Approved for public release; distribution is unlimited

2b DECLASSIFICATION/DOWNGRADING SCHEDULE

SEP 26 1990

4 PERFORMING ORGANIZATION REPORT NUMBER(S)

5 MONITORING ORGANIZATION REPORT NUMBER(S)
AFOSR-TR-

6a NAME OF PERFORMING ORGANIZATION	6b. OFFICE SYMBOL (If applicable)	7a. NAME OF MONITORING ORGANIZATION
Case Western Reserve University		AFOSR/NA

6c ADDRESS (City, State, and ZIP Code)	7b. ADDRESS (City, State, and ZIP Code)
University Circle Cleveland, Ohio 44106	Building 410, Bolling AFB DC 20332-6448

8a NAME OF FUNDING/SPONSORING ORGANIZATION	8b OFFICE SYMBOL (If applicable)	9 PROCUREMENT INSTRUMENT IDENTIFICATION NUMBER
AFOSR/NA	NA	AFOSR 85-0340

8c ADDRESS (City, State, and ZIP Code)	10 SOURCE OF FUNDING NUMBERS			
	PROGRAM ELEMENT NO.	PROJECT NO.	TASK NO	WORK UNIT ACCESSION NO.
Building 410, Bolling AFB DC 20332-6448	61102F	2308	A1	

11 TITLE (Include Security Classification)
(U)
Solid Fuel Combustion

12 PERSONAL AUTHOR(S)
James S. T'ien

13a TYPE OF REPORT	13b. TIME COVERED	14. DATE OF REPORT (Year, Month, Day)	15. PAGE COUNT
Final Report	FROM 8/1/85 TO 10/31/89	August, 1990	78

16 SUPPLEMENTARY NOTATION

17. COSATI CODES			18. SUBJECT TERMS (Continue on reverse if necessary and identify by block number)
FIELD	GROUP	SUB-GROUP	diffusion flame, solid fuel, flame radiation thermophoresis

19 ABSTRACT (Continue on reverse if necessary and identify by block number)

Theoretical analyses were performed on several different types of diffusion flames to study the flame radiation effect. In the first problem, a soot formation and oxidation scheme was incorporated into a turbulent diffusion flame model adjacent to a solid fuel. The computed results for the natural convective fire showed good agreement with experimentally measured solid fuel burning rate. Soot radiation increased its importance with flame height. With flames greater than 1 meter, the radiative heat flux exceeded that by convection. In the second problem, matched asymptotic expansions were employed to study the spherical diffusion flame around a droplet or solid particle with flame radiation. It was found that the importance of radiation increased with droplet radius. The theory predicted that there was a maximum droplet or particle size above which a spherical flame could not be supported due to radiative loss. In the third problem, the thermophoretic motion of small particles (e.g., soot) were studied in a stagnation-point laminar flow next to a heated plate with and without combustion.

(OVER)

20. DISTRIBUTION/AVAILABILITY OF ABSTRACT	21. ABSTRACT SECURITY CLASSIFICATION
☒ UNCLASSIFIED/UNLIMITED ☒ SAME AS RPT. ☒ DTIC USERS	Unclassified

22a NAME OF RESPONSIBLE INDIVIDUAL	22b. TELEPHONE (Include Area Code)	22c. OFFICE SYMBOL
Dr Mitat Birkan	(202) 767-4937	AFOSR/NA

DD Form 1473, JUN 86 Previous editions are obsolete. SECURITY CLASSIFICATION OF THIS PAGE
Unclassified

19. Abstract (continued)

It was found that both the thermophoretic motion and the Brownian particle diffusion can have a profound effect on the particle concentration distributions.

SOLID FUEL COMBUSTION

James S. T'ien
Case Western Reserve University
Cleveland, Ohio 44106

August 1990

Final Report for AFOSR Grant 85-0340
Covering Period August 1, 1985 - October 3, 1989

SOLID FUEL COMBUSTION

James S. T'ien
Case Western Reserve University
Cleveland, Ohio 44106

August 1990

Final Report for AFOSR Grant 85-0340
Covering Period August 1, 1985 - October 3, 1989

Prepared for

AIR FORCE OFFICE OF SCIENTIFIC RESEARCH
Bolling AFB, D. C. 20332-6448

Table of Contents

I. SUMMARY

Theoretical analyses were performed on several different types of diffusion flames to study the flame radiation effect. In the first problem, a soot formation and oxidation scheme was incorporated into a turbulent diffusion flame model adjacent to a solid fuel. The computed results for the natural convective fire showed good agreement with experimentally measured solid fuel burning rate. Soot radiation increased its importance with flame height. When flame length is greater than one meter, the local radiative heat flux exceeded that by convection. In the second problem, matched asymptotic expansions were employed to study the spherical diffusion flame around a droplet or solid particle with flame radiation. It was found that the importance of radiation increased with droplet radius. The theory predicted that there was a maximum droplet or particle size above which a spherical flame could not be supported due to radiative loss. In the third problem, the thermophoretic motion of small particles (e.g., soot) were studied in a stagnation-point laminar diffusion flame. It was found that both the thermophoretic motion and the Brownian particle diffusion can have a profound effect on the particle concentration distributions which in turn will affect the radiative heat transfer.

II. RESEARCH OBJECTIVE

The main objective of this research is to study the effect of flame radiation on diffusion flames, in particular those related to solid and condensed-phase fuels.

III. RESEARCH ACCOMPLISHMENTS

The major accomplishments in the research program will be briefly described in this section. Detailed results are contained in the Appendices and the list of publications.

(A) The Effect of Soot Radiation on the Combustion of Solid Fuels in Turbulent Boundary Layers

The first part of the effort dealt with the adoption of low-Reynolds-number K-ε model for solid fuel burning. In this work, the chemical kinetics are assumed to be infinitely fast and the mixture fraction is assumed to obey a beta probability density distribution. This work shows that the low-Reynolds-number K-ε approach is more physically revealing than the wall function method in analyzing the surface boundary layer problem. By adopting the low-Reynolds-number model where the same equations apply all the way to the wall, we have discovered a number of limitations and problems which are hidden in the wall function approach. To name a few, the equation for mixture fraction is no longer homogeneous, as assumed in all the

previous studies. The evaluation of mean mass fractions for fuel and oxidizer requires certain assumption of small disturbance. The boundary condition for g (square of mixture fraction fluctuation) requires the specification of K (turbulent and kinetic energy) at the wall. With a pyrolyzing solid surface the value of K_w can be an issue. Most details can be found in Publication List No. 1.

In the second part of the effort, finite-rate chemistry was added through an eddy-dissipation model. In addition to convection and diffusive contribution, a soot formation and oxidation scheme is also included in the soot transport equation to compute soot concentration. Radiative heat transfer is calculated by using a two-flux method. The model was applied to the vertical burning of a PMMA slab where there were measured radiation data.

In the step-by-step comparison with experiment, it is found that low-Reynolds-number K-ε turbulence model can produce good heat flux at surface without any modification in pure natural convection along a heated plate. The modification of the low Reynolds number term to accommodate surface mass addition is made in this study. The complete model, when applied to the turbulent wall fire, produces good burning rate, radiant heat flux and average soot volume fraction. The soot radiation is demonstrated to be important in determining the burning rate of solid fuel.

More details can be found in Publication List No. 2, which is attached in Appendix A.

(B) Structure and Extinction of Diffusion Flame with Flame Radiation (Publication List No. 3, Appendix B)

Using droplet combustion as a model problem, and capitalizing on the temperature-sensitive nature of radiative heat transfer, the structure and extinction of diffusion flames with flame radiation is studied via multi-scale activation energy asymptotics. The flame structure analyzed consists of an $O(\varepsilon)$ reaction zone embedded within an $O(\delta)$ radiation zone which in turn is situated on the $O(1)$ diffusive-convective flow field, where $\varepsilon \ll \delta \ll 1$. The analysis yields the structure equation for the reaction zone, which can be cast in the same form as that of Linan's adiabatic diffusion flame problem such that his extinction results can be readily used. Present results show that radiative heat loss promotes flame extinction in general, as expected. Furthermore, it can also lead to the phenomenon of dual extinction turning points in which flame extinction due to reactant leakage and thereby kinetic limitation occurs not only for sufficiently small droplets, as is well established, but also for sufficiently large droplets as a result of excessive heat loss from the correspondingly large flame. Consequently, there exist

diffusive-reactive-radiative systems for which steady combustion is not possible for all droplet sizes. An estimation of the dimensional radiative extinction droplet size is also given for the sample system studied. More details can be found in Publication List No. 3 which is also attached as Appendix B. This work has been collaborated with Dr. B. H. Chao and Professor C. K. Law of Princeton University.

(C) Concentration Distribution of Particles in a Thermophoretically Affected Flow Field

The magnitude of soot radiative emission depends not only on the soot concentration level but also depends on where the soot locations are in the flame (because of different temperature). Therefore the soot particle profile is important for radiative calculation. Since it is known that soot particles are subject to thermophoretic motion in flames, we have undertaken this effort to investigate the effect of thermophoresis and particle Brownian diffusion on particle profiles.

In the first effort, a theoretical analysis is performed to study the distribution of small-size particles in the stagnation-point region of a hot wall (no combustion). Because of the thermophoretic motion, a particle stagnation point is created in the interior of the

flow which can produce singularity when particle diffusion is neglected. By including Brownian diffusion and using matched asymptotic expansions, the structure of the inner diffusion layer near the particle stagnation point is resolved. The results presented in Appendix C illustrate how the diffusion layer is evolved and its structural variation with a number of parameters.

In the second part of the effort, a two-dimensional counterflow diffusion flame stabilized in the forward stagnation region of porous cylinder is analyzed. Fuel is ejected from the cylinder with a specified blowing velocity and diffuses into an oxidizer flow of specified stagnation velocity gradient. In this configuration, particles (e.g., soot) of an assumed average dimension form at a global rate depending on the local fuel concentration and temperature. Thermophoresis gives rise to many different flow patterns for the particles depending on the flame structure and the magnitude of thermophoretic coefficient. In some cases, multiple stagnation points for particle flow exist.

Brownian diffusion needs to be included in this theoretical treatment in order to avoid singular behavior (infinite particle concentration) at the stagnation point under certain conditions. Because the Schmidt number associated with the Brownian diffusion is very large a

special numerical scheme was developed to solve the mass conservation equation for the particles. The numerical scheme was implemented in two stages and allowed to integrate the equation even in situations for multiple turning points (points where particle velocity changes direction). This was achieved by making use of an adaptive mesh refinement scheme.

For cases along the center streamline where the particles are convected toward the stagnation point, a boundary layer behavior is observed. When the product of Prandtl number a the thermophoretic coefficient is greater than a critical value (nearly unity - slightly influenced by chemical kinetics), a local peak of particle concentration is predicted. For cases where particle velocity is from the fuel-rich side toward the flame, the particles, generated in the fuel-rich side (such as soot), can leak through the flame and appear on the fuel-lean side.This can occur only when the stoichiometric fuel-oxidizer mass ratio is less than unity. The detailed profile of particle concentration in counterflow diffusion flames, therefore, depends on many parameters. More details can be found in Publication List No. 5.

IV. PUBLICATIONS

1. D. Y. Shan and J. S. T'ien: Application of Low-Reynolds-Number K-ε Model to Solid Fuel Turbulent Boundary Layer Combustion, AIAA Paper 87-1778 (1987).

2. S. T. Lee and J. S. T'ien: The Effect of Soot Radiation on the Combustion of Solid Fuels, Journal of the Chinese Society of Mechanical Engineers, Vol. 10, No. 4, pp. 243-253 (1989).

3. B. H. Chao, C. K. Law, and J. S. T'ien: Structure and Extinction of Diffusion Flames with Flame Radiation, Twenty-Third Symposium (International) on Combustion, Orleans, France, July, 1990 (In press).

4. N. Ait Messaoudene and J. S. T'ien: Diffusion Layer Structure in a Thermophoretically Affected Flow Over a Hot Surface,Submitted to International Journal of Heat and Mass Transfer.

5. N. Ait Messaoudene and J. S. T'ien: The Effect of Thermophoresis on Particle Distribution in Opposed-Flow Laminar Diffusion Flames, Article in preparation for Combustion Science and Technology.

V. ORAL PRESENTATIONS

1. Application of Low-Reynolds-Number K-ε Model to Solid Fuel Turbulent Boundary Layer Combustion, AIAA/SAE/ASME/ASEE 23rd Joint Propulsion Conference, June 29-July 2, 1987, San Diego, California.

2. The Effect of Soot Radiation on the Combustion of Solid Fuels, AIAA/ASME/SAE/ASEE 24th Joint Propulsion Conference, July 11-13, 1988, Boston, Massachusetts.

3. Structure and Extinction of Diffusion Flames with Flame Radiation, Twenty-Third Symposium (Int.) on Combustion, Orleans, France, July 22-27, 1990.

4. Solid Fuel Combustion, AFOSR Contractor's Meetings, 1986, 1987, 1988, 1989.

VI. PARTICIPATING PROFESSIONALS:

Professor J. S. T'ien: Case Western Reserve University, Principal Investigator

Mr. D. Y. Shan: Ph.D. candidate, Case Western Reserve University

Mr. N. Ait Messaoudene: Ph.D. candidate, Case Western Reserve University

Professor S. T. Lee: Visiting Associate Professor, Case Western Reserve University (on leave from National Taiwan University)

Collaborators:

Dr. B. H. Chao and Professor C. K. Law, Princeton University

Degrees Awarded:

1. D. Y. Shan, Ph.D., 1987

   Thesis title: *Application of Low-Reynolds-Number κ-ε Model to Solid Fuel Turbulent Boundary Layer Combustion.*

2. N. Ait Messaoudene, Ph.D., 1989

   Thesis title: *Concentration Distribution of Particles in a Thermophoretically Affected Flow Field With and Without Combustion.*

Appendix A

中國機械工程學刊第十卷第四期第 243-253 頁（民國七十八年）
Journal of the Chinese Society of Mechanical Engineers, Vol. 10, No. 4, pp. 243-253 (1989)

The Effect of Soot Radiation on the Combustion of Solid Fuels

Shih-Tuen Lee

Department of Mechanical Engineering
National Taiwan University
Taipei, Taiwan, 10764, R.O.C.

James S. T'ien

Department of Mechanical and Aerospace Engineering
Case Western Reserve University
Cleveland, Ohio 44106

Keywords: solid fuel, turbulent combustion, soot, radiation.

ABSTRACT

A comprehensive model for turbulent boundary layer combustion adjacent to solid fuels is established and employed to study the influence of thermal radiation on the burning rate of solid fuels. A low-Reynolds-number two-equation $\kappa - \epsilon$ model is used for flow transport. The treatment of turbulence and chemistry interaction follows the eddy-dissipation model. Radiative heat transfer is calculated by using a two-flux method. In addition to convection and diffusive contribution, the soot formation and oxidation are also included in the soot transport equation to compute the soot concentration.

Comparisons between model calculations and experimental data are carefully carried out for a vertically-burning PMMA fire. Consistent with the experiment results, the model calculation shows that radiation to solid fuel is shown to be the most important factor in determining the solid pyrolysis rate.

烟塵輻射對固體燃料燃燒的效應

李石頓

國立台灣大學機械工程學系

田紹組

凱斯西儲大學機械與太空工程學系

摘 要

本文建立一個描述吸鄰固體燃料的紊流邊界層燃燒之綜合性模式，並利用它研究輻射熱對固體燃料燃燒的影響。在此模式中，流體的流動由一低雷諾數二方程式的 $k - \epsilon$ 模式描述。紊流與化學間交互作用的處理採用渦漩—散逸模式。輻射熱傳則用二通量法計算。烟塵的傳播方程式除了對流及擴散項外，尚包含烟塵的形成及氧化項以便能計算烟塵的濃度。

本文仔細地完成了垂直 PMMA 燃燒時模式計算結果與實驗數據的比較。模式計算結果與實驗結果同樣地顯示出輻射熱是決定固體燃料熱裂解最重要的因素。

INTRODUCTION

In the past decade, a large amount of attention was given to fire study. Detailed experiments [22, 26,6] demonstrated that although convection is the dominant heat transfer mode in small scale fires, radiation heat transfer is the dominant mode in large fires. For the burning of hydrocarbons or polymers, it has long been recognized that soot particles are the important radiation sources in the flame. Recently, it was pointed out [12, 24, 3] that fuel vapors or their decomposition products also play important roles in the flame radiation. Therefore, in order to model the burning behavior of large combustion systems properly, a theoretical model should be able to determine the amount of soot, fuel vapor and combustion product, their distribution in the flame, flame shape and size.

There are many theoretical efforts to model the solid fuel burning rate when radiation is significant. Although these radiation models vary in their complexities, they are all based on very drastic assumptions. For example, in studying turbulent wall fires, two radiation models are assumed by Tamanini [32]. In the first model, radiation power is assumed to be a constant fraction of the energy release rate. In the second model, the radiation is postulated to emit from a thin, constant-temperature layer of particles at the flame front and the value of emissivity of the flame sheet is chosen empirically. In the work of Methochianakis [23], the flame emissivity is assumed to be related to the unburned fuel in an exponential manner. In Ref. 11, radiative heat flux is simply taken as constant mean value.

The purpose of this article is to present a more comprehensive model, compare its calculation with available data and evaluate the importance of soot radiation. This model includes several physical submodels which describe the turbulence phenomena, turbulence-chemistry interaction, radiation heat transfer and the soot formation and oxidation.

MATHEMATICAL MODEL

1. Mean Transport Equation

The physical situation studied is schematically shown in Fig. 1. A turbulent buoyant flame is sustained by the heat feedback to the solid fuel due to convective and radiative heat fluxes from the high temperature gases in the flame. Some assumptions are made for easy treatment of the problem: (a) the average flow is two-dimensional and steady, (b) the binary diffusion coefficients for all pairs of species except soot and soot precursor are equal, (c) mass diffusion due to pressure gradients, temperature gradient are neglected, (d) the soot and soot precursor are treated as minor species, their heat of formation, combustion heat and oxygen

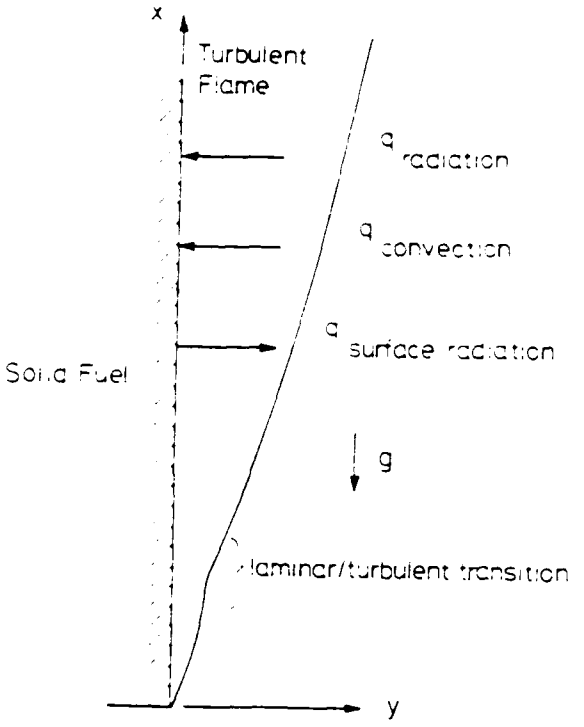

Fig. 1. Schematic of the problem studied

consumption are neglected, (e) the thermophoretic motion of soot is neglected, (f) the specific heat C_p is constant, (g) Lewis numbers except for soot and soot precursor are equal to one, (h) the ideal gas law applies to the gas mixture.

Following the mass-averaging procedure and order of magnitude analysis, the following two-dimensional boundary-layer equations are obtained.

$$\frac{\partial(\bar{\rho}\tilde{u})}{\partial x} + \frac{\partial(\bar{\rho}\tilde{v})}{\partial y} = 0, \tag{1}$$

$$\frac{\partial(\bar{\rho}\tilde{u}\tilde{u})}{\partial x} + \frac{\partial(\bar{\rho}\tilde{v}\tilde{u})}{\partial y} = \frac{\partial}{\partial y}\left[\mu_{eff}\frac{\partial\tilde{u}}{\partial y}\right] + g_x(\bar{\rho} - \bar{\rho}_\infty). \tag{2}$$

$$\frac{\partial(\bar{\rho}\tilde{u}\tilde{Y}_i)}{\partial x} + \frac{\partial(\bar{\rho}\tilde{v}\tilde{Y}_i)}{\partial y} = \frac{\partial}{\partial y}\left[\left(\frac{\mu}{Sc_i} + \frac{\mu_t}{Sc_{i,t}}\right)\frac{\partial\tilde{Y}_i}{\partial y}\right] + \bar{W}_i, \tag{3}$$

$$\frac{\partial(\bar{\rho}\tilde{u}\tilde{h}_t)}{\partial x} + \frac{\partial(\bar{\rho}\tilde{v}\tilde{h}_t)}{\partial y} = \frac{\partial}{\partial y}\left[\left(\frac{\mu}{Pr} + \frac{\mu_t}{Pr_t}\right)\frac{\partial\tilde{h}_t}{\partial y}\right] + \frac{\partial}{\partial y}\left\{\left[\mu_{eff} - \left(\frac{\mu}{Pr} + \frac{\mu_t}{Pr_t}\right)\right]\frac{\partial(1/2\tilde{u}^2 + k)}{\partial y}\right\} + \bar{\rho}g_x\tilde{u} + \dot{S}_R, \tag{4}$$

$$p = \frac{\bar{\rho}R\tilde{T}}{\bar{W}}, \tag{5}$$

where κ is the turbulent kinetic energy and $\dot{S}_R$ is the heat addition due to radiation heat transfer. All the other symbols are described in the Nomenclature.

2. Turbulence Model

Two-equation $\kappa - \epsilon$ model is used to calculate the turbulent viscosity and thus close the averaged equations. Instead of using wall-functions [15] to estimate the transfer of momentum, mass and energy at solid surface, Chien's low-Reynolds-number $\kappa - \epsilon$ model [5] is employed to make the calculation right up to the solid surface. The transport equations for turbulent kinetic energy κ, and the dissipation rate ϵ are:

$$\frac{\partial(\bar{\rho}\tilde{u}\tilde{k})}{\partial x} + \frac{\partial(\bar{\rho}\tilde{v}\tilde{k})}{\partial y} = \frac{\partial}{\partial y}\left[(\mu + \mu_t)\frac{\partial k}{\partial y}\right] + \mu_t\left(\frac{\partial \tilde{u}}{\partial y}\right)^2 - \bar{\rho}\tilde{\epsilon} - 2\mu\frac{k}{y^2}, \tag{6}$$

$$\frac{\partial(\bar{\rho}\tilde{u}\tilde{\epsilon})}{\partial x} + \frac{\partial(\bar{\rho}\tilde{v}\tilde{\epsilon})}{\partial y} = \frac{\partial}{\partial y}\left[(\mu + \frac{\mu_t}{1.3})\frac{\partial \tilde{\epsilon}}{\partial y}\right] + f_1\mu_t\left(\frac{\partial \tilde{u}}{\partial y}\right)^2 - \frac{\tilde{\epsilon}}{k}(f_2 + f_3), \tag{7}$$

where

$$\mu_t = 0.09\left[1 - exp(-C_3 y^+)\right]\frac{\bar{\rho}k^2}{\tilde{\epsilon}}$$

$$f_1 = 1.35\frac{\tilde{\epsilon}}{k}$$

$$f_2 = 1.8\left[1 - 0.22e^{-(R_T/6)^2}\right]\bar{\rho}\tilde{\epsilon}$$

$$f_3 = \frac{2\mu k e^{-0.5y^+}}{y^2}$$

$$R_T = k^2/\nu\tilde{\epsilon}$$

The real turbulent kinetic energy dissipation rate ϵ is related to $\tilde{\epsilon}$ by $\epsilon = \tilde{\epsilon} + 2\nu k/y^2$. In this study, the constant C_3 has been modified from its original value 0.0115 [5] to account for the effect of mass transpiration through the solid surface as

$$C_3 = 0.0115/(1 + \alpha v_w/u^*) \tag{8}$$

This point will be discussed in the later section.

The buoyancy generation terms in the equations (6) and (7) are neglected. Lockwood et al. [18] compared two conventional $\kappa - \epsilon$ turbulence models with and without buoyancy generation terms, they found that, for turbulent round diffusion flame, the results are insensitive to these terms. A application of equations (6) and (7) to natural convection from a vertical isothermal surface also supports this finding. The details are presented in the Results and Discussion Section.

3. Combustion Model

The combustion of fuel is treated as a single step irreversible reaction:

$$1\ \text{Kg [fuel]} + s\ \text{kg [O]} \rightarrow [1 + s]\ \text{kg [product]} \tag{9}$$

The nonlinear interaction between the turbulence and reaction makes the time averaging of the reaction rate very difficult to evaluate. For high local Reynolds-number ($\kappa^2/\nu\epsilon$) region, we assume that the local rate of reaction is limited by the molecular mixing between reactants and follow the approach of Magnussen [21] by expressing the reaction rate as:

$$\bar{\dot{W}}_f = 23.6\bar{\rho}\left(\frac{\nu\epsilon}{k^2}\right)^{1/4}\frac{\epsilon}{\kappa}\min\left[\tilde{Y}_f, \frac{\tilde{Y}_{O2}}{s}\right]\frac{1}{1 - \gamma^*} \tag{10}$$

where

$$\gamma^* = 9.7\left(\frac{\nu\epsilon}{k^2}\right)^{3/4}$$

For low local Reynolds-number region, we assume the reaction rate is chemically controlled and is expressed as [9]:

$$\bar{\dot{W}}_f = A_g\bar{\rho}\tilde{Y}_f\tilde{Y}_{O2}\,e^{-E_g/R\tilde{T}} \tag{11}$$

The criterion of low Reynolds-number is quite arbitrary, Eq. (11) is used when local Reynolds number is less than 50.

4. Soot Model

The processes governing the rates of formation and oxidation of soot are quite complex and quantitative models to describe these processes are not yet fully developed. Quasi-global models [34, 14, 8] have been developed to describe the process of soot formation via a few overall steps. Tesner et al. [34] proposed that soot formation occurs in two steps. The first stage represents formation of radical nuclei (soot precursors); and the second stage the soot particle formation from these nuclei. A modified Tesner's model [10] is adopted in this work. The model describes the formation rate of soot precursor as

$$\frac{d\bar{n}}{dt} = A\tilde{Y}_f exp(-E_n/R\tilde{T}) + (f - g)\bar{n}\frac{\tilde{Y}_f}{Y_{fo}} - g_o\bar{n}(\bar{N} + \bar{n}) \tag{12}$$

and the formation rate of soot as

$$\frac{d\bar{N}}{dt} = g_o\bar{n}(\bar{N} + \bar{n})/K \tag{13}$$

The oxidation of soot is better understood and has been modelled by several investigators [16, 25, 19]. It was suggested that the soot oxidation is chemically controlled in many situations. However Magnussen [20] and Abbas et al. [1] argue that the rate of burning-out

may be controlled by turbulent mixing exspecially in high temperature region. In this study, we follow Abbas et al. and express the burning rate as the smaller of kinetically controlled burning rate $\bar{W}_{s,k}$ and mixing controlled burning rate $\bar{W}_{s,m}$.

$$\bar{W}_{s,c} = \min. [\bar{W}_{s,k}, \bar{W}_{s,m}] \tag{14}$$

where

$$\bar{W}_{s,k} = A_s \frac{P_{O_2}}{\tilde{T}^{1.2}} \exp(-E_s/R\tilde{T}), \tag{15}$$

$$\bar{W}_{s,m} = \frac{\bar{W}_s \tilde{Y}_s}{\tilde{Y}_s} \tag{16}$$

The oxidation of precursors is assumed, following Magnussen's work, as

$$\bar{W}_{n,c} = \frac{\tilde{W}_s \tilde{n}'}{\tilde{Y}_f} \tag{17}$$

where $\tilde{n}'$ is the nucleus particles per unit mass of mixture.

5. Radiation Heat Transfer

The radiation heat transfer is calculated by using two-flux radiation model [30]. The equation for the radiative flux away from the solid surface $\dot{q}^+$ and the radiative flux to the solid surface $\dot{q}^-$ are derived by using Schuster-Schwarzschid method [31]. The resulting equations are:

$$\frac{\partial \dot{q}^+}{\partial y} = -a'\dot{q}^+ + a'E, \tag{18}$$

$$-\frac{\partial \dot{q}^-}{\partial y} = -a'\dot{q}^- + a'F, \tag{19}$$

where a' is the absorption constant and $E = \sigma\tilde{T}^4$. Defining $F = 0.5(\dot{q}^+ + \dot{q}^-)$ and $\dot{q} = \dot{q}^+ - \dot{q}^-$, from Eq. (18) and Eq. (19) we have

$$\frac{\partial}{\partial y}\left(\frac{1}{a'}\frac{\partial F}{\partial y}\right) + a'(E - F) = 0, \tag{20}$$

$$\dot{q} = -\frac{2}{a'}\frac{\partial F}{\partial y} \tag{21}$$

The radiative energy contribution to the source term in the total enthalpy equation is expressed as

$$\dot{S}_R = -\frac{\partial \dot{q}}{\partial y} = 2a'(F - E) \tag{22}$$

The absorption constant $a' = 2K_a$ and the absorption coefficient of the mixture K_a is

$$K_a = 1808\tilde{T}f_v + 20\rho\tilde{Y}_f + (6.2 - 0.00436\tilde{T} + 0.898 \times 10^{-6}\tilde{T}^2)\tilde{Y}_p \tag{23}$$

where f_v is the volume fraction of soot. The contribution of soot to K_a is taken from Ref. 17, the contribution of product is deduced from data of Rapanotti [29], and contribution of fuel vapor is consistent with available data [3].

6. Boundary Conditions

In addition to the equations reported in the previous sections, the specification of boundary conditions is required to complete the mathematical formulation.

At the edge of the boundary layer, we have.

$$\tilde{u} = 0 \tag{24a}$$

$$\tilde{Y}_f = 0 \tag{24b}$$

$$\tilde{Y}_{O_2} = \tilde{Y}_{O_2,\infty} \tag{24c}$$

$$\tilde{h}_t = C_p T_\infty \tag{24d}$$

$$k = 0 \tag{24e}$$

$$\epsilon = 0 \tag{24f}$$

$$\frac{\partial \tilde{Y}_s}{\partial y} = 0 \tag{24g}$$

$$\frac{\partial \tilde{n}'}{\partial y} = 0 \tag{24h}$$

$$F + \frac{1}{a'}\frac{\partial F}{\partial y} = \sigma T_\infty^4 \tag{24i}$$

The boundary conditions at solid surface are:

$$\tilde{u} = 0, \tag{25a}$$

$$\bar{\rho}D_i \frac{\partial \tilde{Y}_i}{\partial y} - (\bar{\rho}\bar{v})\tilde{Y}_i = 0, \text{ for all i except fuel,} \tag{25b}$$

$$\bar{\rho}D_n \frac{\partial \tilde{n}'}{\partial y} - (\bar{\rho}\bar{v})\tilde{n}' = 0, \tag{25c}$$

$$\bar{\rho}D_f \frac{\partial \tilde{Y}_f}{\partial y} - (\bar{\rho}\bar{v})(\tilde{Y}_f - 1) = 0, \tag{25d}$$

$$\tilde{h}_t = q\tilde{Y}_f + C_p T_w + (\bar{v})^2, \tag{25e}$$

$$k = 0, \tag{25f}$$

$$\epsilon = 0, \tag{25g}$$

$$(2 - a_w)\frac{1}{a'}\frac{\partial F}{\partial y}\bar{n} = a_w F - a_w \sigma T_w^4, \tag{25h}$$

$$(\bar{\rho}\bar{v})_w = Bexp(-E_w/RT_w), \tag{25i}$$

$$(\bar{\rho}\bar{v})_w = \frac{\lambda\left(\frac{\partial T}{\partial y}\right)_w + \frac{2}{a'}\frac{\partial F}{\partial y}}{I_s + C_s(T_w - T_{so})}. \tag{25j}$$

The condition (25f) is exact only for rigid wall, for vaporizing wall, this implies negligible burning rate fluctuation. Conditions (25b) - (25d) are obtained from the species mass balance at the solid fuel surface. In condition (25f), it is assumed that the fuel regression rate can be represented in an Arrhenius form. Condition (25h) follows from the relation $\dot{q}^+ = a_w \sigma T_w^4 + (1 - a_w)q^-$ at wall and finally the condition (25j) is obtained from the energy balance at the solid surface.

Numerical Method

The Patankar-Spalding finite difference procedure [27] is chosen for the numerical solution of the system of equations. One hundred and fifty cross stream grid nodes are used to obtain grid-independent solution. Over sixty points are located within $y^+ < 30$. The flow is assumed to start out laminar and the starting profiles are the similarity solutions corresponding to the prescribed burning rate and the radiation flux for constant wall temperature situation. The turbulent calculation is initiated by introducing κ and ϵ at a distance 0.04 m from the leading edge. The initiating profile of κ and ϵ chosen are [32].

$$\kappa = C_k \tilde{u}^2 . \tag{26}$$

$$\epsilon = C_\epsilon k^{3/2} / l \tag{27}$$

where C_k and C_ϵ are constant and

$l = y$ for $y \leq 0.0008$m,

$l = 0.0008$m for $y \geq 0.0008$m

RESULTS AND DISCUSSIONS

The numerical calculation is conducted for PMMA fuel. The physical properties and model constants used in this work are listed in TABLE 1. The viscosity $\mu = 1.4573 \times 10^{-7} \times \tilde{T}^{1.5}/(110.4 + \tilde{T})$ varies with temperature. The constant α in Eq. (8) for the low-Reynolds-number $\kappa - \epsilon$ turbulence model is set to 1.75 in order to get better performance if there is transpiration at the surface. A comparison was made between model calculations and the experimental data [13] in the forced incompressible boundary-layer flow. The results are shown in Fig. 2. In the figure, $G = \dot{m}_w/\rho_\infty U_\infty$ is defined as the mass flux transpired at the solid surface to the mass flux at the free stream. The model performance is good near the wall. Since the velocity-profile at large y^+ is more sensitive to external parameters, particularly the pressure gradient. The deviation at large y^+ for G = 0.0038 may be due to the different pressure gradients used in the numerical caluclation and in the experimental work. The low-Reynolds-number turbulence model was also tested in pure natural convection situation. In the case of buoyant flow near a vertical heated plate, the resulting surface heat flux and

Table I
Values of Properties and Model Constants

Properties or Model Constants	Value	Units
C_p	1254	J Kg^{-1}K
C_s	1463	J Kg^{-1}K
T_{so}	300	°K
T_∞	300	°K
L_s	1.05×10^6	J Kg^{-1}K
σ_w	0.98	
s	1.92	
q	2.5957×10^7	J Kg^{-1}K
$Y_{O_2,\infty}$	0.2315	
D_s	250	A°
ρ_{soot}	2000	Kg/m^3
P_∞	1	atm
A	1.2×10^{41}	part/m^3/s
f-g	100	s^{-1}
Y_{fo}	0.1	
K	2.5	
g_o	1×10^{-15}	m^3/s/part
E_n	180	kcal/mole-°K
Sc_s	10	
Sc_n	10	
Sc_i ($i \neq s,m$)	0.7	
Pr	0.7	
Pr_t	0.9	
Sc_t	0.9	
A_g	5.047×10^7	s^{-1}
E_g	27	kcal/mole-°K
E_w	30	kcal/mole-°K
B	5.144×10^8	Kg/m^2-sec
C_k	0.02	
g_x	−9.8	m/s^2
α	1.75	
A_s	1.302×10^{10}	Kg-°K$^{0.5}$/m^3-atm
E_s	39.3	kcal/mole-°K

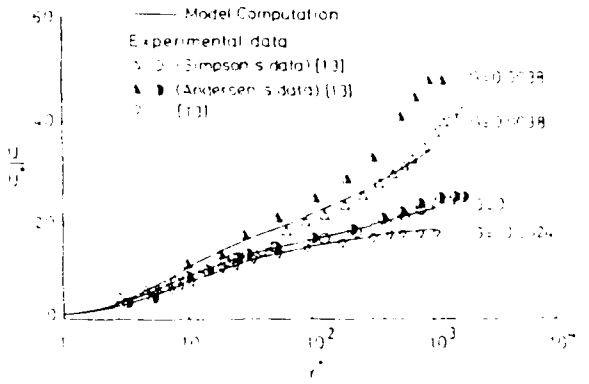

Fig. 2. Velocity profiles with blowing and suction

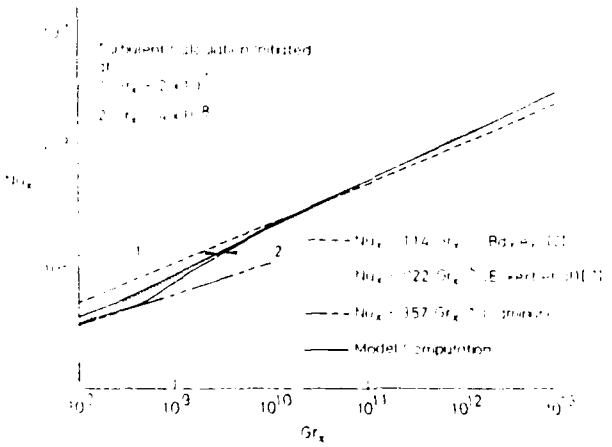

Fig. 3. Local Nusselt number versus Grashof number

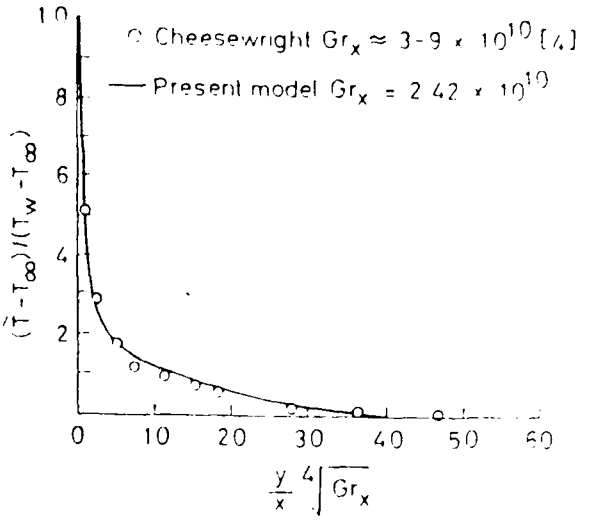

Fig. 4. Temperature profile

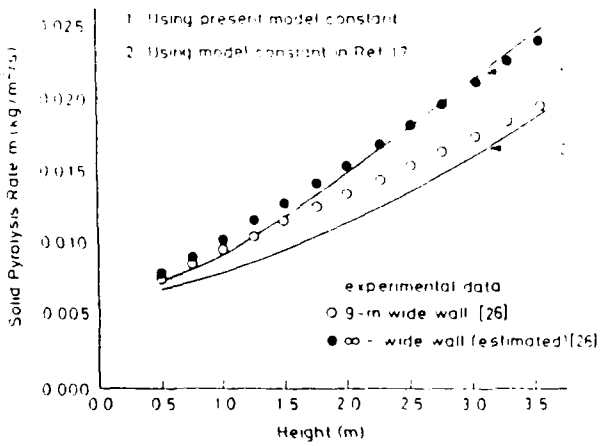

Fig. 5. Pyrolysis rate as a function of height

the temperature profile are shown in Fig. 3 and Fig. 4 respectively. The results are in good agreement with the experimental data and the calculation by Plumb and Kennedy [28] using $\kappa - \epsilon - \overline{T'^2}$ turbulence model which is also a low-Reynolds-number turbulence model but with buoyant generation terms in κ and ϵ equations. This good agreement supports the finding of Lockwood [18] that the buoyant generation terms can be neglected for boundary layer flows with gravity vector nearly perpendicular to temperature gradient. Fig. 3 also indicated that disturbance introduced at different Grashoff number (2×10^7 and 4×10^8) leads to the same result in fully turbulent region.

The complete model was applied to the turbulent buoyant diffusion flame on a vertical surface. Using the soot model constants ($A = 6.25 \times 10^4 0$, $Y_{fo} = 0.2$ and $K = 5$), suggested by the Galant et al. [10], it is found in Fig. 5 that the discrepancy between the predicted and experimental burning rate [26] is large and the calculated averaged volume fraction ($\sim 0.85 \times 10^{-7}$) is much lower than the reported data ($\sim 0.3 \times 10^{-6}$) [6]. This discrepancy may due to the fact that different fuel is burned. The constants suggested by Galant et al. is for methane flame, while the experimental data is obtained by burning PMMA. Using the constants shown in Table 1, we could make the calculated burning rate quite close to the experimental data and the calculated average soot volume fraction ($\sim 0.27 \times 10^{-6}$) agrees with the reported data.

Fig. 6 shows the ratio of radiant heat flux to the surface to the total heat flux. It indicates that the radiation heat transfer is a dominant heat transfer mode in a big fire. The calculated radiant heat flux and convective heat flux to the surface are also compared with the results of Orloff et al. [26] in Fig. 7. Orloff et al. deduced the radiant heat flux and the convective heat flux from experimental data using optically thin flame analysis. The radiant heat flux using the gray flame analysis is also presented in Fig. 7. From Fig. 7, we can see that the agreement between the model calculation and the results of Orloff et al. is good. The calculated convective heat flux decreases slightly with the height, while the radiant heat flux increases with the height. The decrease of the convective heat flux is due to the decrease of gas temperature. As will be shown in

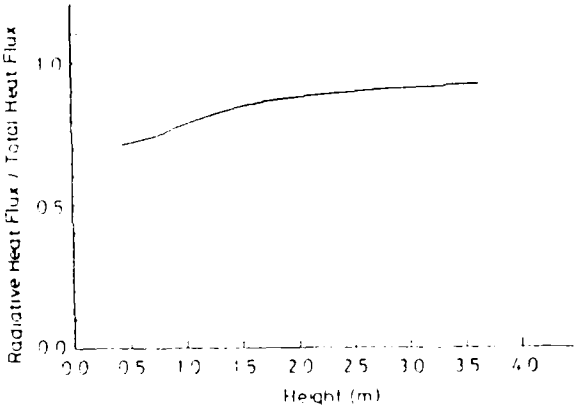

Fig. 6. Radiative contribution to total heat flux to the surface

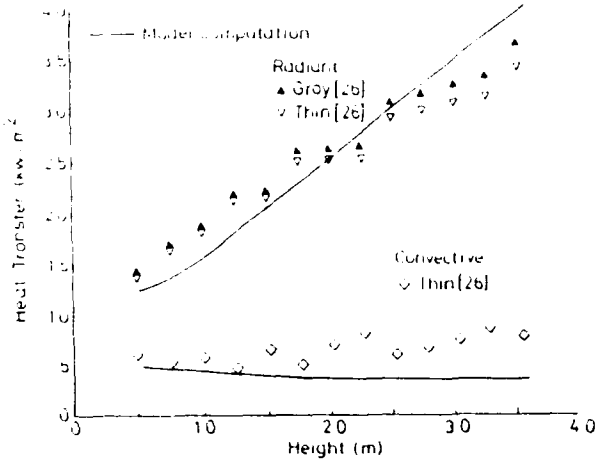

Fig. 7. Radiant and convective heat transfer to the surface versus height

parametric studies, the convective heat flux increases slightly in no-gas-phase-radiation case even the flame temperature decreases slightly with the height. Radiation in gas phase makes the gas temperature decreases more and it is this further decrease of gas temperature that makes the convective heat flux decrease instead increase slightly with the height. The increase of radiant heat is mainly due to the fact that the soot volume fraction increases with height.

Fig. 8 and Fig. 9 show the typical profiles of velocity, temperature, fuel mass fraction, oxygen mass fraction, soot mass fraction, turbulent kinetic energy and dissipation rate. The soot mass fraction is much larger on the fuel-rich side than on the fuel-lean side. It is consistent with the experimental finding that the soot layer is on the fuel side of the flame zone. Because of the shape of velocity profile, the turbulent kinetic energy and the turbulent energy dissipation profiles have dents near the peak of the velocity profile. As shown in Fig. 10, further downstream, the turbulent kinetic energy profile shows two local maximum values.

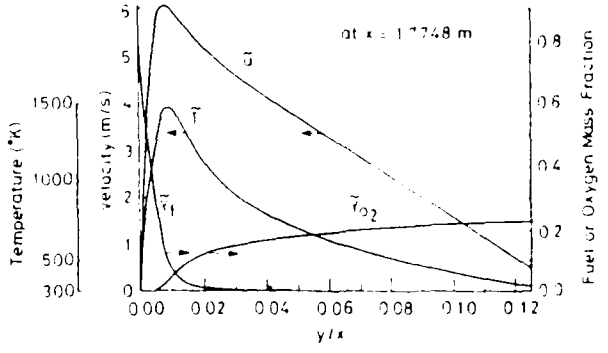

Fig. 8. Profiles of velocity, temperature, fuel mass fraction and oxygen mass fraction

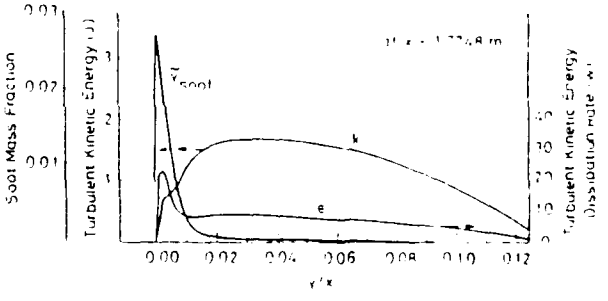

Fig. 9. Profiles of soot, turbulent kinetic energy and turbulent kinetic energy dissipation rate

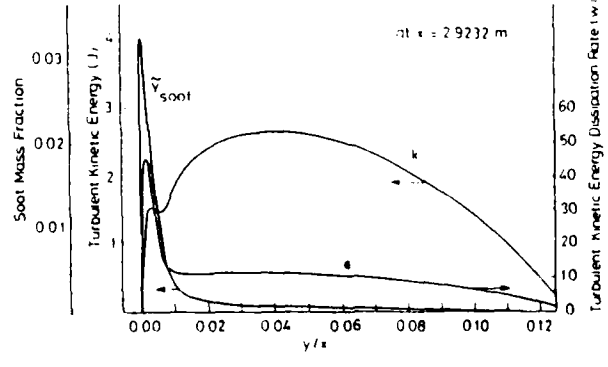

Fig. 10. Profiles of soot, turbulent kinetic energy and turbulent kinetic energy dissipation rate

Parametric studies are also presented in Fig. 11. Two additional cases are considered: one without fuel contribution in gas-phase radiation, and the other without gas-phase radiation at all but still with surface radiation. We note that the radiant heat transfer from soot is large compared with that from fuel vapor. The figure also indicates that in the no-gas-phase-radiation case, the burning rate increases slightly with height. In this case the heat flux to the surface is totally due to the convection, so the convective heat flux increases with height. The reason why the convective heat flux increases with height is that the gas velocity, the boundary

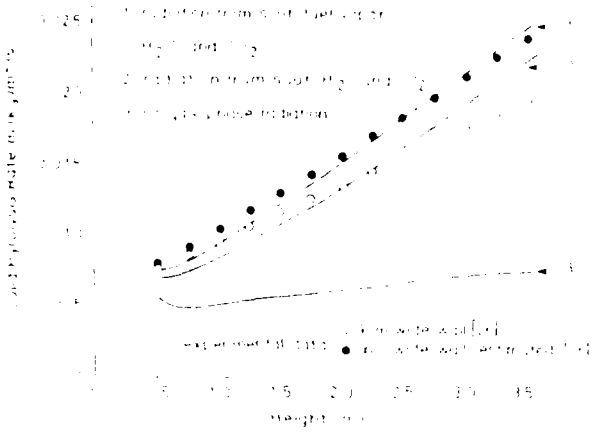

layer thickness and therefore the turbulent diffusivity increase with height. It is not due to the flame temperature but the temperature profile, because the maximum gas temperature decreases slightly with height.

In numerical calculation, it is found that the transition from laminar region to fully turbulent region is quite sensitive to the triggering method. Fig. 12 shows some results. In all calculations the initial turbulent kinetic energy is kept the same but the initial dissipation rate varies. The figure indicates that depending on the initial disturbance, the laminar-turbulent transition point varies. We note that the curves are nearly parallel to each other at fully turbulent region and shift from each other. This shift is due to the variation of the laminar-turbulent transition point. Partial support for this is that in fully developed region, at same local burning rate, they (except C_ϵ = 0.3 which is still in early turbulent region) all nearly have the same boundary layer thickness. The possibility of using low-Reynolds-number $\kappa - \epsilon$ turbulence model to calculate the transition region and also the influence of the initial disturbance is still under study. At the present stage, the transition portion only provides a means of leading to the fully developed turbulent region which is of interest.

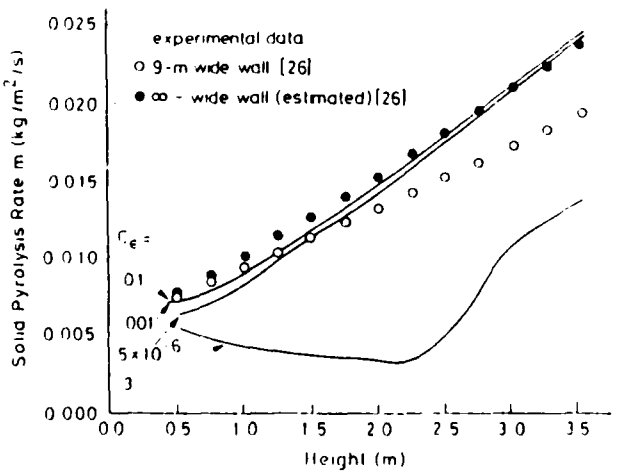

Fig. 12. Pyrolysis rate as a function of height

CONCLUSIONS

The pyrolysis and combustion of solid fuel in a turbulent boundary layer are determined by the complex interaction of various transport and kinetic processes. In order to assess the relative importance of each component process, a comprehensive model which consists of several sub-models is established in this work. Although simple expressions are given to the sub-model processes, the combined model is quite complex. Because the only existing experiment on solid fuel burning in turbulent flame with detailed measurement of radiative properties is in natural convection, the model is first validated in this situation.

In the step-by-step comparison with experiment, it is found that Chien's low-Reynolds-number $\kappa - \epsilon$ turbulence model can produce good heat flux at surface without any modification in pure natural convection along heated plate. The modification of the low Reynolds number term to accommodate surface mass addition is made in this study. The complete model, when applied to the turbulent wall fire, produces good burning rate, radiant heat flux and average soot volume fraction. The soot radiation is demonstrated to be important in determining the burning rate of solid fuel.

The prediction of diffusion flame in a turbulent boundary layer depends on the upstream conditions which are usually difficult to specify completely. In the present study, a laminar-to-turbulent transition procedure is adopted. But the results also depend on how the triggering disturbance is specified. The determination of the most proper triggering disturbance in the low-Reynolds-number $\kappa - \epsilon$ turbulence model to bridge the laminar and turbulent regions will need more work.

ACKNOWLEDGMENT

This research is supported by AFOSR Grant 85-0340. S. T. Lee would like to acknowledge the support of ICOMP and NSC of R.O.C.

NOMENCLATURE

A	Model constant
A_g	Preexponential constant
A_s	Preexponential constant
a'	Absorption constant
a_w	Emissivity of solid fuel
B	Preexponential constant
C_k	Coefficient

C_p Specific heat of the mixture
C_s Specific heat of the solid fuel
C_ϵ Coefficient
D Species diffusivity
D_s Soot particle diameter
E $= \sigma \tilde{T}^4$
E_g Activation energy
E_n Activation energy
E_s Activation energy
E_w Activation energy
F $= 0.5 (\dot{q}^+ + \dot{q}^-)$
f Model constant
f_v Volume fraction of soot
G $= \dot{m}_w \rho_\infty U_\infty$
Gr Local Grashof number
g Model constant
g_o Model constant
g_x Acceleration of gravity in x direction
h_t Total enthalpy
K Model constant
K_a Absorption coefficient of the mixture
k Turbulent kinetic energy
L_s Latent heat of the solid fuel
l Length
$\dot{m}$ Mass flux
N Concentration of soot particle (part/m_3)
n Nucleus concentration (part/m_3)
n' $= n/\rho$
P pressure
P_r Prandtl number
P_{r_t} Turbulent Prandtl number
q Heat of combustion per unit of mass of fuel
$\dot{q}$ $= \dot{q}^+ - \dot{q}^-$
$\dot{q}^+$ Radiative heat flux in positive y direction
$\dot{q}^-$ Radiative heat flux in negative y direction
R Universal gas constant
s Stoichiometric oxidizer/fuel mass ratio
Sc_i Schmidt number of species i
$Sc_{i,t}$ Turbulent Schmidt number of species i
$\dot{S}_R$ Heat addition due to radiation heat transfer
T Temperature
T_w Surface temperature
T_∞ Ambient temperature
T_{so} Bulk temperature of the solid fuel
t Time
u Velocity in the x direction
u^* $= (\tau_w/\rho)^{1/2}$
u^+ $= u/u^*$
v Velocity in the y direction
$\overline{W}$ Mean molecular weight
$\overline{\dot{W}}_i$ Neat rate of formation of species i per unit volume
$\overline{\dot{W}}_{n,c}$ Rate of consumption of nuclei per unit
$\overline{\dot{W}}_{s,c}$ Rate of consumption of soot per unit volume
$\overline{\dot{W}}_{s,k}$ Rate of consumption of soot per unit volume controlled by chemical kinetics
$\overline{\dot{W}}_{s,m}$ Rate of comsumption of soot per unit volume controlled by mixing
x Coordinate along the wall
Y_{fo} Model constant
Y_i Mass fraction of species i
y coordinate normal to the wall
y^+ $= yu^*/\nu$
α Model constant
γ^* Mass fraction occupied by fine structures
ϵ Rate of dissipation of turbulent kinetic energy
$\dot{\epsilon}$ $= \epsilon - 2k\nu/y^2$
λ Thermal conductivity
μ Molecular dynamic viscosity
μ_t Turbulent viscosity
μ_{eff} $= \mu + \mu_t$
ν Molecular kinetic viscosity
ρ Density
σ Planck constant
τ_w Wall shear stres

Superscripts

$-$ Conventional time mean value
$\sim$ Favre mean value

Subscripts

f fuel
i species i
o_2 Oxygen
n Nucleus

p	product
s	soot
t	turbulence
w	Wall
∞	Ambience

REFERENCES

1. Abbas, A.S. and Lockwood, F.C.: Note, "Prediction of Soot Concentration in Turbulent Diffusion Flames", Journal of the Institute of Energy, pp. 112-115 (1985).
2. Bayley, F.J., "An Analysis of Turbulent Free-Convection Heat Transfer", Proc. Inst. Mechanical Engineers, VOL. 169, No. 20, pp. 361 (1955).
3. Brosmer, M.A. and T'ien, C.L., "Thermal Radiation Properties of Propylene", *Combustion Science and Technology*, 48, pp. 163-175 (1986).
4. Cheesewright, R., "Turbulent Natural Convection From a Vertical Plane Surface", Journal of Heat Transfer, VOL. 11, pp. 397-406 (1968).
5. Chien, K.Y., "Prediction of Channel and Boundary-Layer Flows with Low-Reynolds-Number Turbulence Model", AIAA Journal, 20, pp. 23-38 (1982).
6. De Ris, J., "Fire Radiation – A Review", *17th International Symposium on Combustion*, The Combustion Institute, pp. 1003 (1979).
7. Eckert, E.R.G. and Jackson, T.W., "Analysis of Turbulent Free Convection Boundary Layer on a Flat Plate", NACA Technical Note 2207 (1950).
8. Farmer, F., Edelman, R., Wong, E., "Modelling Soot Emissions in Combustion Systems", General Motors Symposium on Particle Carbon Formation During Combustion (1980).
9. Foutch, D.W. and T'ien, J.S.: Extinction of a Stagnation-Point Diffusion Flame at Reduced Gravity, AIAA Journal, Vol. 25, pp. 1972 (1987).
10. Galant, S., Grouset, D., Martinez, G., Micheau, P., and Allemand, J.B., "Three-Dimensional Steady Parabolic Calculations of Large Scale Methane Turbulent Diffusion Flames to Predict Flare Radiation Under Cross Wind Conditions", *20th International Symposium on Combustion*, The Combustion Institute, pp. 531 (1984).
11. Joulain, P., et al., "Influence of Coupled Convection, Conduction and Radiation Heat Transfer on the Burning of Plastics", *17th International Symposium on Combustion*, The Combustion Institute, pp. 1041 (1979).
12. Kashiwagi, T., "Radiative Ignition Mechanism of Solid Fuels", *Fire Safety Journal*, 3, pp. 1185-200 (1981).
13. Kays, W.M. and Moffat, R.J., "The behavior of Transpired Turbulent Boundary Layers", Studies in Convection, Vol. 1: Theory, Measurement and Application, Academic Press, London, (1975).
14. Khan, I.M. and Greeves, G., "A Method for Calculating the Formation and Combustion of Soot in Diesel Engines", *Heat Transfer in Flames*, Scripta Book Co. (1974).
15. Launder, B.E. and Spalding, D.B., *Mathematical Models of Turbulence*, Academic Press (1972).
16. Lee, K.B., Thring, M.W. and Beer, J.M., "On the Rate of Combustion of Soot in a Laminar Soot Flame", *Combustion and Flame*, 6, pp. 137-145 (1962).
17. Lee, K.Y., Zhong, Z.Y., and T'ien, C.L., "Blockage of Thermal Radiation by Soot Layer in Combustion of Condensed Fuels", *20th International Symposium on Combustion*, The Combustion Institute, pp. 1629 (1984).
18. Lockwood, F.C. and Stolakis, P., "Assessment of two turbulence models for turbulent round diffusion jets with combustion", *Fourth Symp. on Turbulent shear flows*, Karlsruhe, FR German (1983).
19. Maahs, H.G., "Oxidation of Carbon at High Temperature-Reaction-Rate Control or Transport Control," NASA TND-6310 (1971).
20. Magnussen, B.F., "Modelling of Reaction Processes in Turbulent Flames with Special Emphasis on Soot Formation and Combustion", General Motors Symposium on Particle Carbon Formation During Combustion (1980).
21. Magnussen, B.F., "On the Structure of Turbulence and a Generalized Eddy Dissipation Concept for Chemical Reactions in Turbulent Flow", 19th AIAA Aerospace Science Meeting, St. Louis (1981).
22. Markstein, G.H., "Radiative Energy Transfer from Gaseous Diffusion Flames", *15th International Symposium on Combustion*, The Combustion Institute, pp. 1284 (1975).
23. Metochianakis, M.E. and Netzer, D.W., "Modeling Solid-Fuel Ramjet Combustion, Including Radiation to the Fuel Surface", *Journal of Spacecraft*, Vol. 20, No. 4, pp. 1405 (1983).
24. Modak, A.T., "The Burning of Large Pool Fires", *Fire Safety Journal*, 3, pp. 177-184 (1981).
25. Nagle, J. and Strickland-Constable, R.F., "Oxidaton of Carbon Between 1000 – 2000°C", *Proc. of the Fifth Carbon Conference*, pp. 154-164 (1962).
26. Orloff, L., Modak, A.T. and Alpert, R.L., "Burning of Large-Scale Vertical Surfaces", *16th International Symposium on Combustion*, The Combustion Institute, pp. 1345 (1977).
27. Patankar, S.V. and Spalding, D.B. "Heat and Mass Transfer in Boundary Layers", Intertext Books, London (1970).
28. Plumb, O.A. and Kennedy, L.A., "Application of a κ ϵ Turbulence Model to Natural Convection from a Vertical Isothermal Surface", *Journal of Heat Transfer*, pp. 79 (1977).
29. Rapanotti, J.L. and Brzustowski, T.A., "A New Approach to Modelling Radiation from Open Flames", *Combustion Science and Technology*, VOL. 49, pp. 251 (1986).
30. Sidall, R.G. and Selcuk, N., "Two-Flux Modelling of Two-Dimensional Radiative Transfer in axi-

symmetrical Furnaces", *Journal of Institute of Fuel XLIX*, 10 (1976)

31 Siegel, R. and Howell, J.R., *Thermal Radiation Heat Transfer*, 2nd Edition, McGraw-Hill, New York (1981)

32 Lamamm, F., "A Numerical Model for the Prediction of Radiation-Controlled Turbulent Wall Fires", *17th International Symposium on Combustion*, The Combustion Institute, pp. 1075-1086 (1979)

33 Lamamm, F., Ahmad, T., "Modeling of Buoyant Turbulent Flames Over Combustible Walls", Proc. of the 7th Int. Coll. on Gasdynamics of Explosions and Reactive Systems, Gottingen (1979)

34 Lesner, P.A., Snegirova, E.D., and Knotre, V.G., "Kinetics of Dispersed Carbon Formation", *Combustion and Flame*, 17, pp. 253-260 (1971)

Paper Received: February, 1989
Accepted: May, 1989
Author for Correspondence: Shih-Tuen Lee

Appendix B

Twenty-Third Symposium (International)
on Combustion
Orleans, France
July 22 - 27, 1990

STRUCTURE AND EXTINCTION OF DIFFUSION FLAMES WITH FLAME RADIATION

B. H. Chao and C. K. Law
Department of Mechanical and Aerospace Engineering
Princeton University
Princeton, New Jersey 08544

J. S. T'ien
Department of Mechanical and Aerospace Engineering
Case Western Reserve University
Cleveland, Ohio 44106

ABSTRACT

Using droplet combustion as a model problem, and capitalizing on the temperature-sensitive nature of radiative heat transfer, the structure and extinction of diffusion flames with flame radiation is studied via multi-scale activation energy asymptotics. The flame structure analyzed consists of an $O(\varepsilon)$ reaction zone embedded within an $O(\delta)$ radiation zone which in turn is situated in the $O(1)$ diffusive-convective flow field, where $\varepsilon \ll \delta \ll 1$. The analysis yields the structure equation for the reaction zone, which can be cast in the same form as that of Liñán's adiabatic diffusion flame problem such that his extinction results can be readily used. Present results show that radiative heat loss promotes flame extinction in general, as expected. Furthermore, it can also lead to the phenomenon of dual extinction turning points in which flame extinction due to reactant leakage and thereby kinetic limitation occurs not only for sufficiently small droplets, as is well established, but also for sufficiently large droplets as a result of excessive heat loss from the correspondingly large flame. Consequently there exist diffusive-reactive-radiative systems for which steady combustion is not possible for all droplet sizes. An estimation of the dimensional radiative extinction droplet size is also given for the sample system studied.

1. INTRODUCTION

The seminal paper of Liñán[1] provides a complete and definitive analysis of the structure of quasi-one-dimensional diffusion flames with a one-step irreversible reaction. The flame structure and response are found to be mainly described by a Damköhler number, Da, defined as the ratio of the characteristic flow time to the characteristic reaction time. The Burke-Schumann flame sheet is attained in a distinguished limit of infinite Da. With continuous decrease in Da, the characteristic extinction turning-point behavior is exhibited, yielding a distinct lower limit in Da beyond which steady burning is not possible. This limit is therefore identified as the extinction Damköhler number, $Da_{E,K}$. The cause of extinction is excessive reactant leakage through the flame.

The system analyzed by Liñán is a conservative one in that in the flame-sheet limit the flame temperature is the adiabatic flame temperature, T_f^*. The analysis therefore neglects an inherent nonadiabatic feature of flame processes, namely radiative heat loss from the flame. While quantitatively it is clear that radiative heat loss is expected to reduce the flame temperature and promote extinction, there is also a subtle, qualitative feature which has not been adequately recognized and studied. That is, since radiative heat loss is a volume phenomenon, the extent of loss and thereby reduction in the flame temperature are expected to increase with increasing system dimension. Since Da frequently also increases with increasing system dimension and thereby residence time, the effect of radiative heat loss should then increase with increasing Da. When such a loss becomes excessive, the reduction in flame temperature could again cause extinction. Thus it is possible that, in addition to the existence of a lower limit in Da, namely $Da_{E,K}$, which characterizes extinction of a nonradiative or slightly radiative flame, there could also exist an upper limit in Da, say $Da_{E,R}$, which characterizes the maximum amount of heat loss the flame can sustain for steady burning, and therefore can be termed as a radiative extinction Damköhler number. The subtlety here is that since chemical reactivity and radiative loss both increase with increasing Da, it is not clear a priori whether and when radiative loss can be sufficiently strong to dominate over chemical enhancement to cause extinction.

The possibility that an upper and a lower bound in Da can exist was suggested by T'ien[2] and Sibulkin[3] from their numerical solutions of the stagnation and free-convection diffusion flames

respectively. Radiative loss in these cases is from the surface. The problem of diffusion flame extinction with flame radiation was analyzed by Sohrab et al.[4] for the counterflow configuration by using activation energy asymptotics. A criterion for flame extinction was presented, although the extinction turning point behavior of interest here was not explicitly displayed. Furthermore, while reactant leakage is essential for diffusion flame extinction, with or without radiative heat loss, this analysis has suppressed reactant leakage by assuming complete reaction.

The objective of the present study is therefore to provide a rigorous analysis of the structure and extinction of diffusion flames with flame radiation. The results demonstrate conclusively the existence of the dual extinction boundaries of $Da_{E,K}$ and $Da_{E,R}$. The analysis is conducted via the model problem of droplet combustion for its simple configuration as well as ready conceptual identification of either the droplet or the flame diameter as the characteristic system dimension.

2. FORMULATION

2.1 Governing Equations

The problem to be analyzed, shown as the inset in Fig. 1, is the quasi-steady, isobaric, spherically-symmetric droplet combustion, with second-order Arrhenius kinetics, in a given oxidizing environment. Overall mass conservation yields the constant mass evaporation rate, $m=4\pi r^2 \rho u$, where r is the radial distance, ρ the density, and u the radial velocity.

For the radiative heat loss, recognizing that the heat loss rate per unit volume, $\dot{q}_R$, is a highly sensitive function of temperature, following Sohrab et al.[4] we approximate $\dot{q}_R$ by an Arrhenius-type function

$$\dot{q}_R = 4\sigma\kappa T^4 \approx B_R \exp(-T_{a,R}/T) \quad ,$$

where $\sigma = 1.36\times10^{-8}$ cal/m^2-sec-K^4 is the Stefan-Boltzmann constant, κ the Planck's mean absorption coefficient, B_R a pre-exponential rate parameter and $T_{a,R}$ an "activation temperature" for radiative loss.

With conventional transport property assumptions (see, for example, Ref. 5), the nondimensional conservation equations for energy and species are

$$\frac{1}{\tilde{r}^2}\frac{d}{d\tilde{r}}\left(\tilde{m}\tilde{T}-\tilde{r}^2\frac{d\tilde{T}}{d\tilde{r}}\right)=Da\,(\tilde{\rho}/\tilde{T}_f)^2\tilde{Y}_F\tilde{Y}_O\exp(-\tilde{T}_{a,K}/\tilde{T})-Ra\exp(-\tilde{T}_{a,R}/\tilde{T})\quad,\tag{2.1}$$

$$\frac{1}{\tilde{r}^2}\frac{d}{d\tilde{r}}\left(\tilde{m}\tilde{Y}_i-\tilde{r}^2\frac{d\tilde{Y}_i}{d\tilde{r}}\right)=-Da\,(\tilde{\rho}/\tilde{T}_f)^2\tilde{Y}_F\tilde{Y}_O\exp(-\tilde{T}_{a,K}/\tilde{T})\quad,\quad i=F,O\quad,\tag{2.2}$$

with the boundary conditions

$$\tilde{r}=1\ :\ \tilde{T}=\tilde{T}_s\ ,\ d\tilde{T}/d\tilde{r}=\tilde{m}\tilde{q}_v\ ,\ \tilde{m}\tilde{Y}_F-(d\tilde{Y}_F/d\tilde{r})=\tilde{m}\ ,\ \tilde{m}\tilde{Y}_O-(d\tilde{Y}_O/d\tilde{r})=0\ ;\tag{2.3a}$$

$$\tilde{r}\to\infty\ :\ \tilde{T}\to\tilde{T}_\infty\ ,\ \tilde{Y}_F\to 0\ ,\ \tilde{Y}_O\to\tilde{Y}_{O,\infty}\ .\tag{2.3b}$$

The various nondimensional quantities are given by

$$\tilde{T}=\frac{T}{q_F/c_p}\ ,\ \tilde{Y}_F=Y_F\ ,\ \tilde{Y}_O=Y_O/\left(\frac{\nu_O W_O}{\nu_F W_F}\right)\ ,\ \tilde{r}=r/r_s\ ,\ \tilde{m}=\frac{m}{4\pi r_s\lambda/c_p}\ ,\ \tilde{\rho}=\rho/\rho_f\ ,$$

$$\tilde{q}_v=q_v/q_F\ ,\ \tilde{T}_{a,K}=\frac{T_{a,K}}{q_F/c_p}\ ,\ \tilde{T}_{a,R}=\frac{T_{a,R}}{q_F/c_p}\ ,\ Da=\frac{\nu_O B_K p^2 c_p^3 r_s^2}{W_F q_F^2 R^2\lambda}\ ,\ Ra=\frac{B_R r_s^2 c_p}{\lambda q_F}\ ,$$

where the subscripts s and f respectively denote quantities at the droplet surface and flame sheet. In the above T is the temperature, Y_i the mass fraction of species i, λ the thermal conductivity, c_p the specific heat at constant pressure, D the mass diffusion coefficient, q_F the heat of combustion per unit mass of fuel, ν_i the stoichiometric coefficient, W_i the molecular weight, B_K the pre-exponential factor, $T_{a,K}$ the activation temperature, p the pressure, R the gas constant, q_v the latent heat of vaporization at temperature T_s, and the subscripts F and O respectively denote fuel and oxidizer. The equation of state $\rho T=p/R$ is also applied.

Using Eq. (2.2), a coupling function $(\tilde{Y}_F-\tilde{Y}_O)$ can be obtained, yielding an explicit relation between $\tilde{Y}_F$ and $\tilde{Y}_O$,

$$\tilde{Y}_O=\tilde{Y}_F-1+(1+\tilde{Y}_{O,\infty})\exp(-\tilde{m}/\tilde{r})\ .\tag{2.4}$$

The problem is now reduced to solving the mass burning rate $\tilde{m}$ as well as the remaining conservation equations for $\tilde{Y}_F$ and $\tilde{T}$.

2.2 Discussions on Limiting Situations

Several limits can be discussed based on the values of $\tilde{T}_{a,K}$, $\tilde{T}_{a,R}$, Da and Ra. First, in the limit of $\tilde{T}_{a,R}\to\infty$ with Ra fixed, we retrieve the adiabatic droplet combustion case. Similarly, for $\tilde{T}_{a,K}\to\infty$ and

Da fixed, we have pure droplet vaporization in a radiative environment. The simultaneous requirement of both of the above limits yields the case of droplet vaporization in a nonradiative environment.

We next take the distinguished limit of $\tilde{T}_{a,K} \to \infty$ and $Da \to \infty$ for the reaction zone. For $\tilde{T}_{a,R} \to \infty$ with Ra fixed, radiative heat loss is frozen and we retrieve the classical adiabatic droplet flame-sheet combustion limit. If we in addition take the distinguished limit $\tilde{T}_{a,R} \to \infty$ and $Ra \to \infty$ for the radiative heat loss, then we obtain the nonadiabatic flame-sheet situation. The problem, however, is not closed at the limit, as demonstrated in the Appendix. Thus broadening of the radiation zone is an inherent feature of a radiative diffusion flame.

We next consider situations in which one or both of $\tilde{T}_{a,K}$ and $\tilde{T}_{a,R}$ are finite. Since both the reaction and radiative loss processes are temperature sensitive, we have $\tilde{T}_{a,K} \gg 1$ and $\tilde{T}_{a,R} \gg 1$. Concerning the relative orders of $\tilde{T}_{a,K}$ versus $\tilde{T}_{a,R}$, the situation of $\tilde{T}_{a,R} \gg \tilde{T}_{a,K}$ is of no interest because radiative loss is frozen. On the other hand the reverse situation of $\tilde{T}_{a,K} \gg \tilde{T}_{a,R} \gg 1$ is clearly of physical relevance. Here a thin reaction zone of $O(\varepsilon)$ thickness is embedded within a somewhat thicker, $O(\delta)$, radiation zone which, however, is still much thinner than the entire flow field of dimension O(1), as shown in the inset of Fig. 1. This is the situation to be analyzed in the next section.

The situation of $\tilde{T}_{a,R} = O(\tilde{T}_{a,K})$ is not studied because it is analytically more complex, as pointed out in Sohrab et al.[4] Its behavior is expected to be intermediate between those of the $\tilde{T}_{a,K} \gg \tilde{T}_{a,R}$ and $\tilde{T}_{a,K} \ll \tilde{T}_{a,R}$ situations, representing the transition between them. Details of the transition, however, could be interesting and merit further study.

We now present the asymptotic analysis of droplet combustion with flame radiation.

3. ASYMPTOTIC SOLUTION

3.1 Outer Solution

In the limit of $\tilde{T}_{a,K} \gg 1$, chemical reaction occurs only in a thin region of $O(\varepsilon)$ around the location of maximum temperature. In the outer regions bounded away from this reaction zone, chemical reaction is frozen because of the reduced temperature. Since the flow here is influenced by two singularities of

$O(\varepsilon)$ and $O(\delta)$ respectively, the properties must be expanded through both ε and δ. Thus the proper expansion of the properties, for example the mass burning rate $\tilde{m}$, is

$$\tilde{m} = [\,\tilde{m}_0 + \varepsilon\,\tilde{m}_1 + O(\varepsilon^2)\,] + \delta\,[\,\tilde{m}_2 + \varepsilon\,\tilde{m}_3 + O(\varepsilon^2)\,] + O(\delta^2)\ , \tag{3.1}$$

where the $O(\varepsilon^m)$ and $O(\delta^n)$ terms are the corrections due to finite-rate kinetics and radiative heat loss respectively.

In the presence of radiative heat loss, the outer solutions of $\tilde{Y}_F$ and $\tilde{T}$ do not take the same form and therefore need to be separately analyzed.

<u>3.1a Solution for $\tilde{Y}_F$</u> - Substituting the expansion of $\tilde{Y}_F$, in a form similar to that of Eq. (3.1), into the nonreactive limit of Eq. (2.2), and solving subject to the boundary conditions in Eq. (2.3), we obtain

$$1 < \tilde{r} < \tilde{r}_f : \quad \tilde{Y}_{F,0}^- = 1 - b_0^- \exp(-\tilde{m}_0/\tilde{r})\ , \tag{3.2a}$$

$$\tilde{Y}_{F,j}^- = -[\,b_j^- - (\,b_0^-\tilde{m}_j/\tilde{r}\,)\,]\exp(-\tilde{m}_0/\tilde{r})\ , \quad j=1,2\ ; \tag{3.2b}$$

$$\tilde{r}_f < \tilde{r} < \infty : \quad \tilde{Y}_{F,0}^+ = b_0^+\,[\,1 - \exp(-\tilde{m}_0/\tilde{r})\,]\ , \tag{3.2c}$$

$$\tilde{Y}_{F,j}^+ = b_j^+ - [\,b_j^+ - (\,b_0^+\tilde{m}_j/\tilde{r}\,)\,]\exp(-\tilde{m}_0/\tilde{r})\ , \quad j=1,2\ , \tag{3.2d}$$

where the b's are the integration constants to be determined.

It is important to recognize that while heat loss is not explicitly present in the conservation equation for $\tilde{Y}_F$, $\tilde{Y}_F$ is affected by heat loss through its influence on the mass burning rate $\tilde{m}$.

<u>3.1b Solution for $\tilde{T}$</u> - In order to properly solve for the temperature distribution in the outer regions, we need to first separately analyze the radiation and radiatively-frozen zones and then match their solutions. In the frozen zone, energy transport is characterized by convection-diffusion balance. The temperature fields are expanded in the manner of Eq. (3.1) which, when substituted into Eq. (2.1) and solved subject to the relevant boundary conditions in Eq. (2.3), yields

$$1 < \tilde{r} < \tilde{r}_f : \quad \tilde{T}_0^- = \tilde{T}_s - \tilde{q}_v + \tilde{q}_v \exp\{\tilde{m}_0[\,1-(1/\tilde{r})\,]\}\ , \tag{3.3a}$$

$$\tilde{T}_j^- = \tilde{q}_v\tilde{m}_j[\,1-(1/\tilde{r})\,]\exp\{\tilde{m}_0[\,1-(1/\tilde{r})\,]\}\ , \quad j=1,2\ ; \tag{3.3b}$$

$$\tilde{r}_f < \tilde{r} < \infty : \quad \tilde{T}_0^+ = \tilde{T}_\infty + a_0^+[\,1-\exp(-\tilde{m}_0/\tilde{r})\,]\ , \tag{3.3c}$$

$$\tilde{T}_j^+ = a_j^+ - [\,a_j^+ - (\,a_0^+\tilde{m}_j/\tilde{r}\,)\,]\exp(-\tilde{m}_0/\tilde{r})\ , \quad j=1,2\ , \tag{3.3d}$$

where the a's are the integration constants to be determined.

In the radiation region of $O(\delta)$, the coordinate is stretched as $\zeta = (\tilde{r} - \tilde{r}_f)/\delta$ while the proper temperature expansion is

$$\tilde{T} = \tilde{T}_f - \delta [\, \Theta_1 + (\varepsilon / \delta)\, \Theta_2 + \varepsilon \Theta_3 + \cdots] + O(\delta^2) \quad . \tag{3.4}$$

Substituting Eq. (3.4) and ζ into the chemically-frozen form of Eq. (2.1) and expanding, we obtain

$$d^2\Theta_1^{\pm} / d\zeta^2 = -\tilde{\mathrm{Ra}} \exp(-\Theta_1^{\pm}) \quad , \tag{3.5a}$$

$$d^2\Theta_j^{\pm} / d\zeta^2 = -\tilde{\mathrm{Ra}}\, \Theta_j^{\pm} \exp(-\Theta_1^{\pm}) \quad , \quad j = 2, 3 \quad , \tag{3.5b}$$

where the small expansion parameter δ is defined as $\delta = \tilde{T}_f^2 / \tilde{T}_{a,R}$ while

$$\tilde{\mathrm{Ra}} = \delta\, \mathrm{Ra} \exp(-\tilde{T}_{a,R} / \tilde{T}_f) \tag{3.6}$$

is a reduced parameter representing radiative heat loss. Thus energy conservation in the radiation region is diffusion-radiation balanced.

Matching the solutions in the radiation and frozen regions as $\tilde{r} \to \tilde{r}_f$ yields

$$\tilde{T}_f = \tilde{T}_s - \tilde{q}_v + \tilde{q}_v \exp\{\tilde{m}_0 [\, 1 - (1 / \tilde{r}_f)\,]\} \quad , \quad a_0^+ = (\tilde{T}_f - \tilde{T}_\infty) / [\, 1 - \exp(-\tilde{m}_0 / \tilde{r}_f)\,] \quad , \tag{3.7}$$

and the boundary conditions needed to solve Eqs. (3.5) as $\zeta \to \pm\infty$, giving

$\zeta < 0$:

$$\Theta_1^- = 2 \ln \left| 1 - [\, \tilde{\mathrm{Ra}} / (2 g_0^2)\,] \exp(g_0 \zeta + g_1) \right| - g_0 \zeta - g_1 \quad , \tag{3.8a}$$

$$\Theta_2^- = -(\tilde{T}_f - \tilde{T}_s + \tilde{q}_v)(\tilde{m}_1 / g_0)[\, 1 - (1 / \tilde{r}_f)\,][\, g_0^2 + 2\, \tilde{\mathrm{Ra}} \exp(-\Theta_1^-)\,]^{1/2} \quad , \tag{3.8b}$$

$$\frac{d\Theta_3^-}{d\zeta} = -g_0 \tilde{m}_1 \left(1 + \frac{1}{\tilde{m}_0} - \frac{1}{\tilde{r}_f} \right) \frac{1 + (\tilde{\mathrm{Ra}} / g_0)\, \zeta \exp(g_0 \zeta + g_1) - \{[\, \tilde{\mathrm{Ra}} / (2 g_0^2)\,] \exp(g_0 \zeta + g_1)\}^2}{\{1 - [\, \tilde{\mathrm{Ra}} / (2 g_0^2)\,] \exp(g_0 \zeta + g_1)\}^2} \quad ; \tag{3.8c}$$

$\zeta > 0$:

$$\Theta_1^+ = 2 \ln \left| 1 - [\, \tilde{\mathrm{Ra}} / (2 h_0^2)\,] \exp(h_1 - h_0 \zeta) \right| + h_0 \zeta - h_1 \quad , \tag{3.9a}$$

$$\Theta_2^+ = -\{(a_1^+ / h_0)[\, 1 - \exp(-\tilde{m}_0 / \tilde{r}_f)\,] + (\tilde{m}_1 \tilde{r}_f / \tilde{m}_0)\}\, [\, h_0^2 + 2\, \tilde{\mathrm{Ra}} \exp(-\Theta_1^+)\,]^{1/2} \quad , \tag{3.9b}$$

$$\frac{d\Theta_3^+}{d\zeta} = \{\, a_1^+ (\tilde{m}_0 / \tilde{r}_f^2) \exp(-\tilde{m}_0 / \tilde{r}_f) + h_0 \tilde{m}_1 [\, (1 / \tilde{m}_0) - (1 / \tilde{r}_f)\,]\,\} \times$$

$$\frac{1 - (\tilde{\mathrm{Ra}} / h_0)\, \zeta \exp(h_1 - h_0 \zeta) - \{[\, \tilde{\mathrm{Ra}} / (2 h_0^2)\,] \exp(h_1 - h_0 \zeta)\}^2}{\{1 - [\, \tilde{\mathrm{Ra}} / (2 h_0^2)\,] \exp(h_1 - h_0 \zeta)\}^2} \quad , \tag{3.9c}$$

where

$$g_0 = (\tilde{T}_f - \tilde{T}_s + \tilde{q}_v) \tilde{m}_0 / \tilde{r}_f^2 \quad , \quad h_0 = (\tilde{T}_f - \tilde{T}_\infty) (\tilde{m}_0 / \tilde{r}_f^2) \exp(- \tilde{m}_0 / \tilde{r}_f) / [1 - \exp(- \tilde{m}_0 / \tilde{r}_f)] \quad ,$$

$$g_1 = (\tilde{T}_f - \tilde{T}_s + \tilde{q}_v) \tilde{m}_2 [1 - (1 / \tilde{r}_f)] \quad , \quad h_1 = a_2^+ [1 - \exp(- \tilde{m}_0 / \tilde{r}_f)] + (h_0 \tilde{r}_f \tilde{m}_2 / \tilde{m}_0) \quad . \tag{3.10}$$

3.2 Inner Solution

In the reaction region of $O(\varepsilon)$ thickness, the temperature is within an $O(\varepsilon)$ reduction from the maximum temperature $\tilde{T}_f$. The stretched spatial coordinate is $\xi = (\tilde{r} - \tilde{r}_f)/\varepsilon$ while the temperature and fuel distributions are expanded as

$$\tilde{T} = \tilde{T}_f - \varepsilon [\theta_1 + O(\delta) + O(\varepsilon / \delta) + \cdots] - \varepsilon^2 [\theta_2 + O(\delta) + O(\varepsilon / \delta) + \cdots] + O(\varepsilon^3) \tag{3.11}$$

$$\tilde{Y}_F = \varepsilon [\phi_1 + O(\delta) + O(\varepsilon / \delta) + \cdots] + \varepsilon^2 [\phi_2 + O(\delta) + O(\varepsilon / \delta) + \cdots] + O(\varepsilon^3) \quad . \tag{3.12}$$

Since oxidizer concentration is also an $O(\varepsilon)$ quantity in this thin region, substitution of Eq. (3.12) into Eq. (2.4) and forcing the leading order term to vanish yields

$$\tilde{r}_f = \tilde{m}_0 / \ln(1 + \tilde{Y}_{O,\infty}) \quad . \tag{3.13}$$

Substituting Eqs. (3.11) and (3.12) as well as the stretched coordinate ξ into Eqs. (2.1) and (2.2), and expanding, we have two source-free equations expressing the local coupling functions and a third equation with the source term representing chemical reaction,

$$\frac{d^2}{d\xi^2} (\theta_1 - \phi_1) = 0 \quad , \tag{3.14}$$

$$\frac{d^2}{d\xi^2} (\theta_2 - \phi_2) + \frac{2}{\tilde{r}_f} \frac{d}{d\xi} \left[\xi \frac{d}{d\xi} (\theta_1 - \phi_1) \right] - \frac{\tilde{m}_0}{\tilde{r}_f^2} \frac{d}{d\xi} (\theta_1 - \phi_1) = 0 \quad , \tag{3.15}$$

$$\frac{d^2\theta_1}{d\xi^2} = \tilde{Da}\, \phi_1 [\phi_1 - (\tilde{m}_1 / \tilde{r}_f) + (\tilde{m}_0 / \tilde{r}_f^2) \xi] \exp(- \theta_1) \quad , \tag{3.16}$$

where the small parameter ε is defined as $\varepsilon = \tilde{T}_f^2 / \tilde{T}_{a,K}$ and

$$\tilde{Da} = \varepsilon^3 (Da / \tilde{T}_f^2) \exp(- \tilde{T}_{a,K} / \tilde{T}_f) \tag{3.17}$$

is a reduced Damköhler number. In obtaining Eq. (3.16), we have also used $\tilde{\rho} = 1 + O(\varepsilon)$.

Equations (3.14) to (3.16) show that this region is reactive-diffusive. Radiative heat loss is not important here because its volume is much smaller than the total volume of the radiation region.

3.3 Final Solution

The boundary conditions required to solve Eqs. (3.14) to (3.16) are derived from matching the inner

and outer solutions as $\tilde{r} \to \tilde{r}_f$ for $\tilde{Y}_F$ and $\zeta \to 0$ for $\tilde{T}$. Upon matching, we first obtain $b_0^- = 1 + \tilde{Y}_{O,\infty}$, $b_0^+ = 0$ and the solutions for $\tilde{m}_2$, $a_2^\pm$ and $b_2^\pm$. Next, the boundary conditions for the inner equations as $\xi \to \pm\infty$ are also obtained. Integrating Eq. (3.14) twice and Eq. (3.15) once, and applying the proper boundary conditions, we obtain

$$(g_0^2 + 2\tilde{R}a)^{1/2} + (h_0^2 + 2\tilde{R}a)^{1/2} = \tilde{m}_0 / \tilde{r}_f^2 \quad , \tag{3.18}$$

and two additional relations to express $b_1^\pm$ in terms of a_1^+ and $\tilde{m}_1$. With these relations, ϕ_1 can be expressed in terms of θ_1 as

$$\phi_1 = \{ \theta_1 + [\tilde{m}_1 / \ln(1 + \tilde{Y}_{O,\infty})] - \xi \} (h_0^2 + 2\tilde{R}a)^{1/2} \quad . \tag{3.19}$$

Substituting Eq. (3.19) into Eq. (3.16) yields a second order, nonlinear ordinary differential equation with θ_1 as the only unknown, subject to the matching conditions obtained. This equation needs to be solved numerically.

The problem can be considered to be completely solved at this stage in that all parameters to the lowest orders needed to solve the problem are either determined or are determinable through straightforward numerical integration. The solution includes three expressions, Eqs. (3.7), (3.13) and (3.18), which define the three bulk combustion properties of the flame temperature $\tilde{T}_f$, the flame-sheet location $\tilde{r}_f$, and the mass burning rate $\tilde{m}_0$, in terms of the system, kinetic and radiation parameters. Furthermore, solution of the differential equation Eq. (3.16), with ϕ_1 given by Eq. (3.19), determine the parameters a_1^+ and $\tilde{m}_1$ and consequently the condition for flame extinction.

4. RESULTS AND DISCUSSIONS

4.1 Re-Scaling

The solutions just obtained are not amenable for ready interpretation of the system behavior because the quantifying parameters δ, ε, $\tilde{R}a$ and $\tilde{D}a$ are all functions of the leading-order flame temperature $\tilde{T}_f$, which in turn depends on the characteristics of radiative heat loss. It is therefore necessary to re-scale all the parameters to a fixed, absolute reference state. Failure to do so could lead to spurious interpretation of the results.

The obvious choice of the reference state is the adiabatic state. Designating properties of this

state by the superscript *, we have

$$\tilde{T}_f^* = [\,\tilde{T}_\infty + \tilde{Y}_{O,\infty}(\,1 - \tilde{q}_v + \tilde{T}_s\,)\,] / (\,1 + \tilde{Y}_{O,\infty}\,) \quad , \tag{4.1}$$

$$\tilde{m}_0^* = \ln\{\,1 + [\,(\,\tilde{T}_\infty + \tilde{Y}_{O,\infty} - \tilde{T}_s\,) / \tilde{q}_v\,]\,\} \quad , \tag{4.2}$$

$$\tilde{r}_f^* = \tilde{m}_0^* / \ln(\,1 + \tilde{Y}_{O,\infty}\,) \quad . \tag{4.3}$$

The parameters referred to this adiabatic, reference state can then be expressed as

$$\tilde{Da}^* = \varepsilon^{*3}\, Da \exp(-\tilde{T}_{a,K} / \tilde{T}_f^*) / \tilde{T}_f^{*2} \quad , \quad \varepsilon^* = \tilde{T}_f^{*2} / \tilde{T}_{a,K} \quad ,$$

$$\tilde{Ra}^* = \delta^*\, Ra \exp(-\tilde{T}_{a,R} / \tilde{T}_f^*) \quad , \quad \delta^* = \tilde{T}_f^{*2} / \tilde{T}_{a,R} \quad . \tag{4.4}$$

With the expressions in Eq. (4.4), the system dependent parameters can be rewritten as

$$\tilde{Da} = \tilde{Da}^*\,(\,\tilde{T}_f / \tilde{T}_f^*\,)^4 \exp[\,\tilde{T}_{a,K}(\,\tilde{T}_f^{*-1} - \tilde{T}_f^{-1}\,)\,] \quad , \tag{4.5}$$

$$\tilde{Ra} = \tilde{Ra}^*\,(\,\tilde{T}_f / \tilde{T}_f^*\,)^2 \exp[\,\tilde{T}_{a,R}(\,\tilde{T}_f^{*-1} - \tilde{T}_f^{-1}\,)\,] \quad , \tag{4.6}$$

while $a_1^+ = (\tilde{T}_f^*/\tilde{T}_f)^2 a_1^{+*}$ is obtained from $\varepsilon a_1^+ = \varepsilon^* a_1^{+*}$ and a similar expression can be obtained for $\tilde{m}_1$.

Since Da and Ra, and hence $\tilde{Da}^*$ and $\tilde{Ra}^*$, vary with the droplet size in the same, quadratic, manner, we can define a parameter $\Gamma = \tilde{Ra}^* / \tilde{Da}^*$, which is the ratio representing the characteristic reaction time to the characteristic radiation time. It depends only on the kinetic and radiation constants of the system.

In addition to the need for re-scaling to an absolute reference state, it is also necessary to clearly identify the roles of the various dependent and independent parameters in their dimensional and nondimensional forms. Of particular importance is the droplet size, r_s, which has been extensively used in nondimensionalization. For example, an increase in the (reduced) Damköhler number $\tilde{Da}^*$ can be interpreted as either an increase in chemical reactivity or an increase in the droplet size. Similarly, an increase in the heat loss parameter $\tilde{Ra}^*$ can imply either an increase in the loss intensity or an increase in the droplet size. Thus a clear measure of the relative influence of reaction and radiation is the parameter Γ, in which the droplet size is divided out. The problem is defined by using any two of the three parameters $\tilde{Da}^*$, $\tilde{Ra}^*$ and Γ.

It is further found that the final structure equation of the present system can be converted to that of Liñán[1] by re-scaling the various parameters and variables as

$$\tilde{\theta} = \alpha^{1/3}\theta_1 - \gamma\eta \quad , \quad \alpha = 4\,\tilde{Da}^{*}\,(\tilde{T}_f/\tilde{T}_f^{*})^4\,[\tilde{r}_f/\ln(1+\tilde{Y}_{O,\infty})]^2 \exp[\tilde{T}_{a,K}(\tilde{T}_f^{*\,-1} - \tilde{T}_f^{-1})] \quad ,$$

$$\eta = (\alpha^{1/3}/2)\,[\xi \ln(1+\tilde{Y}_{O,\infty}) - \tilde{m}_1]/\tilde{r}_f \quad , \quad \gamma = 1 - [2\tilde{r}_f/\ln(1+\tilde{Y}_{O,\infty})]\,(g_0^2 + 2\tilde{Ra})^{1/2} \quad .$$

The structure equation, Eq. (3.16), is then reduced to that of Liñán, given by

$$\frac{d^2\tilde{\theta}}{d\eta^2} = (\tilde{\theta}^2 - \eta^2)\exp[-\alpha^{-1/3}(\tilde{\theta}+\gamma\eta)] \quad ; \quad \left(\frac{d\tilde{\theta}}{d\eta}\right)_{-\infty} = -1 \quad , \quad \left(\frac{d\tilde{\theta}}{d\eta}\right)_{\infty} = 1 \quad . \tag{4.7}$$

The quantities $\tilde{a}$ and $\tilde{m}_1^{*}$ can be determined from solving Eq. (4.7) as

$$\tilde{a} = -a_1^{+\,*}\tilde{Y}_{O,\infty}/(1+\tilde{Y}_{O,\infty}) = \alpha^{-1/3}(\tilde{T}_f/\tilde{T}_f^{*})^2\,[h_0/(h_0^2 + 2\tilde{Ra})^{1/2}] \lim_{\eta\to\infty}(\tilde{\theta}-\eta) \quad , \tag{4.8}$$

$$\tilde{m}_1^{*} = -\{\alpha^{-1/3}\ln(1+\tilde{Y}_{O,\infty})/[\tilde{r}_f(g_0^2 + 2\tilde{Ra})^{1/2}]\}(\tilde{T}_f/\tilde{T}_f^{*})^2 \lim_{\eta\to-\infty}(\tilde{\theta}+\eta) \quad . \tag{4.9}$$

Equation (4.7) has been numerically solved by Liñán.[1] Results show that extinction is expected for $\alpha < \alpha_E$, where α_E is approximately given by

$$\alpha_E = e\,[(1-|\gamma|) - (1-|\gamma|)^2 + 0.26\,(1-|\gamma|)^3 + 0.055\,(1-|\gamma|)^4] \tag{4.10}$$

with very good accuracy. It may be noted that in the presence of radiative heat loss, γ varies with α through $\tilde{Da}^{*}$ for fixed Γ and therefore cannot be independently specified.

We mention in passing that Sohrab et al.[4] assumed complete reaction so that there is no reactant leakage through the flame. This means that in addition to the required boundary conditions to solve Eq. (4.8), the additional constraints $(\tilde{\theta}+\eta)_{-\infty} = (\tilde{\theta}-\eta)_{\infty} = 0$ are applied, which renders the problem over-determined.

4.2 Results

To demonstrate the salient features of the solution, the combustion of a heptane droplet at its boiling temperature and burning in the standard atmosphere is solved. The system parameters adopted are

$$T_s = 372\,K \quad , \quad T_\infty = 298\,K \quad , \quad T_{a,K} = 22{,}000\,K \quad , \quad T_{a,R} = 8{,}000\,K \quad , \quad c_p = 0.317\,cal/gm\text{-}K \quad ,$$

$$q_F = 10.8\,kcal/gm \quad , \quad q_v = 75.8\,cal/gm \quad , \quad (\nu_O W_O)/(\nu_F W_F) = 3.52 \quad , \quad Y_{O,\infty} = 0.232 \quad .$$

We first present the flame characteristics when the reaction zone is infinitely thin and reactant leakage is suppressed. The flame is still of finite thickness due to radiation broadening. The

combustion parameters $\tilde{T}_f$, $\tilde{m}_0$, and $\tilde{r}_f$ are given by the three algebraic expressions Eqs. (3.7), (3.13) and (3.18), which can be iteratively solved together with the scaling relation Eq. (4.6).

Figure 1 shows the flame temperature $\tilde{T}_f$ and mass burning rate $\tilde{m}_0$ as functions of $\tilde{Ra}^*$. The flame radius $\tilde{r}_f$ is not shown because it is directly proportional to $\tilde{m}_0$. It is seen that $\tilde{T}_f$ and $\tilde{m}_0$ both decrease with increasing $\tilde{Ra}^*$. Thus for a fixed droplet radius r_s, increasing radiative loss intensity reduces the flame temperature and mass burning rate, as expected. However, if we interpret the increase in $\tilde{Ra}^*$ as due to an increase in r_s, with fixed radiation parameters, then we should also account for the fact that the physical burning rate m_0 varies linearly with r_s. Then the numerical values show that m_0 still increases with r_s, albeit at a slower rate in the presence of radiative loss.

Since the reaction rate is assumed to be infinitely fast, extinction is not described at this level of solution. Consequently Fig. 1 does not exhibit the extinction turning point behavior. To allow for finite-rate kinetics, Eq. (4.7) is solved numerically. Figure 2 plots $\bar{a}$ versus $\tilde{Da}^*$ for several values of $\tilde{Ra}^*$, where $\bar{a}$ represents the temperature reduction due to incomplete reaction and is directly related to the amount of fuel leakage through the flame.

We first discuss the adiabatic limit, $\tilde{Ra}^*=0$, which corresponds to $\gamma=0.867$ for the present system. This is the situation studied by Liñán.[1] It is seen from Fig. 2 that there exists a minimum $\tilde{Da}^*$, $\tilde{Da}^*_{E,K}$, such that there is no solution for $\tilde{Da}^* < \tilde{Da}^*_{E,K}$ and there are two solutions for $\tilde{Da}^* > \tilde{Da}^*_{E,K}$. Thus $\tilde{Da}^*_{E,K}$ can be identified as a (reduced) kinetic extinction Damköhler number. The lower branch, which shows $\bar{a}$ decreases with increasing $\tilde{Da}^*$, is the physically realistic solution.

To investigate the influence of radiative heat loss, it is important to specify the process/parameter which is held fixed in the comparison. To demonstrate this point, in Fig. 2 the effect of radiation is exhibited by plotting $\bar{a}$ versus $\tilde{Da}^*$ on constant $\tilde{Ra}^*$. Since both $\tilde{Da}^*$ and $\tilde{Ra}^*$ depend on the droplet size through r_s^2, r_s^2 should be considered as a fixed quantity in the comparison. Figure 2 then shows that, for a given reference reactivity $\tilde{Da}^*$, increasing radiative loss through $\tilde{Ra}^*$ increases the extent of reactant leakage. This is reasonable because of the reduction in the flame temperature and thereby reaction rate due to the heat loss. The kinetic extinction Damköhler number is consequently also increased. By the same reasoning, we see that for a given radiative loss $\tilde{Ra}^*$, increasing reactivity

$\tilde{Da}^*$ reduces the extent of leakage.

Figure 2 is relevant for studying the effects of changing the fuel/oxidizer system (e. g. fuel substitution, oxidizer enrichment) on a droplet of fixed size. However, frequently a more relevant question to ask is the effect of varying the droplet size for a fixed fuel/oxidizer system. For example, after a fuel droplet or particle has achieved ignition, the droplet size r_s will steadily decrease although its physical flame size r_f can first increase, due to fuel vapor accumulation,[5] and then decrease. The relevant plot to demonstrate droplet size effects is again $\bar{a}$ versus $\tilde{Da}^*$, but on constant Γ, as shown in Fig. 3. For such a plot we can consider the reference chemical reactivity to be fixed. Thus for a given $\tilde{Da}^*$, increasing Γ increases the influence of radiation, while for a fixed Γ increasing $\tilde{Da}^*$ implies increasing values of r_s.

Figure 3 shows that, for smaller values of $\tilde{Da}^*$, the flame response is qualitatively similar to that of Fig. 2, exhibiting the turning point behavior at $\tilde{Da}^*_{E,K}$. The behavior, however, becomes qualitatively different for larger values of $\tilde{Da}^*$. It is seen that by continuously increasing $\tilde{Da}^*$ along the lower branch of a constant Γ curve, the reactant leakage first decreases and then increases until another turning point is encountered. According to our earlier discussion and anticipation, this turning point should represent an alternate mode of extinction, namely extinction due to fuel leakage in the presence of excessive radiative heat loss and flame temperature reduction for large droplet sizes. We therefore designate this critical state as that of the radiation extinction Damköhler number, $\tilde{Da}^*_{E,R}$. It may be emphasized that this mode of extinction is caused by the slow kinetics due to the heat loss but not the loss itself. Thus steady burning is possible only for $\tilde{Da}^*_{E,K} < \tilde{Da}^* < \tilde{Da}^*_{E,R}$. This range in $\tilde{Da}^*$ is further diminished with increasing Γ (Fig. 3) such that there exists a maximum Γ, say Γ_c, beyond which burning is absolutely not possible, for the fuel/oxidizer system, regardless of the droplet size.

In Fig. 4 we have plotted the extinction Damköhler number $\tilde{Da}^*_E$ and the corresponding flame temperature as a function of Γ. This curve can be generated directly by using Eq. (4.10) with the proper definitions of α and γ. Thus for a given Γ, the possible values of $\tilde{Da}^*$ are bounded by the upper and lower branches of this curve, which respectively represent the kinetic and radiative extinction Damköhler numbers $\tilde{Da}^*_{E,K}$ and $\tilde{Da}^*_{E,R}$. The maximum value of Γ is found to be $\Gamma_c = 0.0302$ for this model

system. It is also seen that the flame temperature reduction is small for the upper, kinetic extinction regime, but is substantially larger for the lower, radiative extinction regime, as is reasonable to expect.

It is of interest to estimate the characteristic radiative extinction droplet size. Such an estimation requires values of λ and B_R. For λ we used 2.97×10^{-4} cal/cm-sec-K, which is that of air at 2,000K. To estimate B_R, we first fitted T^4 in the temperature range of $1{,}600K \le T \le 2{,}500K$ to yield $T^4 = 8.90\times10^{14}\exp(-8{,}000K/T)\ K^4$. Next, the Planck's mean absorption coefficient is taken as the molar averaged value of the mixture in the radiation region. Since the amount of reactants is small compared to that of the products in this region, it is reasonable to consider that the mixture consists of CO_2, H_2O and N_2. Furthermore, since N_2 is very non-radiative as compared to CO_2 and H_2O, we have $\kappa \approx x_{CO_2}\kappa_{CO_2} + x_{H_2O}\kappa_{H_2O}$. Using[6] $\kappa_{CO_2} = 5.63\times10^{-2}\ cm^{-1}$ and $\kappa_{H_2O} = 7.13\times10^{-3}\ cm^{-1}$ evaluated at 1 atm and 2,000K, and $x_{CO_2} = 0.124$ and $x_{H_2O} = 0.142$ for the stoichiometric burning of heptane in air, we obtain $\kappa = 8.00\times10^{-3}\ cm^{-1}$. Using κ, σ and the fitted T^4, B_R is determined as 3.87×10^3 cal/m^3-sec and consequently $\tilde{Ra}^* = (28.2\ m^{-2})r_s^2$ with $\tilde{T}_f^*$ calculated from Eq. (4.1).

Experimentally, n-alkane droplets burning in air typically extinguish, in the kinetic limit, in the range around $r_{s,E,K} \approx 0.1$ mm. This yields $\tilde{Ra}^*_{E,K} = 2.82\times10^{-7}$. Using this value and the relation $\tilde{Da}^*_{E,K} = \tilde{Ra}^*_{E,K}/\Gamma$, Fig. 4 shows that there is no solution even with the maximum Γ of 0.0302. Therefore the flame cannot exist at all. This result obviously contradicts experimental observations because n-alkane droplets can be routinely burned in room air. The cause of this discrepancy is believed to be the excessively large flame size predicted by the theory. That is, it is well established[5] that because of the unity Lewis number assumption and the neglect of the fuel vapor accumulation process, the classical d^2-law solution, which is the leading order solution in the present problem, predicts flamefront standoff ratios for n-alkane droplet combustion in air to be typically 40. Experimentally[5] the ratio is more in the range of 5 to 10. This large theoretical flame size then leads to excessive radiative heat loss and thereby promotes radiation-induced extinction. Since radiative heat loss scales with r_f^2, this effect can be approximately accounted for by reducing $\tilde{Ra}^*_{E,K}$ by the square of the ratio of the experimental to the theoretical flame size. If we take this ratio to be, say 6, then through iteration we find $\tilde{Da}^*_{E,K} = 4.67\times10^{-7}$ and $\Gamma = 0.0167$, which yields a radiative extinction droplet size of

$r_{s,E,R}$ = 0.93 mm. This value is about 10 times larger than the kinetic extinction droplet size. It is reasonable to expect that in the presence of soot the value of $r_{s,E,R}$ could be further reduces to render radiative extinction an important process in heterogeneous combustion.

5. CONCLUDING REMARKS

In the present study we have successfully analyzed the structure and extinction characteristics of diffusion flames suffering radiative heat loss from the flame, when the thickness of the radiation zone is asymptotically intermediate of those of the reaction zone and the bulk flow field. Perhaps the most interesting result from the present study is the identification of the existence of dual turning points. Specifically, by fixing the thermochemical aspects of a fuel/oxidizer system, we have shown that steady droplet burning is possible only for droplet sizes within a certain range. Extinction of smaller droplets is caused by purely finite-rate kinetics, while extinction of larger droplets is caused by excessive radiative heat loss which eventually again leads to the kinetic limitation. The range of droplet size for steady burning narrows with increasing radiation intensity, as represented by the parameter Γ, such that droplet burning is not possible beyond a certain critical Γ_C.

Extension of the present results to other quasi-one-dimensional flow configurations is straightforward, involving primarily changes in the definitions for Da and Ra to account for the different expressions of residence times.

Acknowledgements

This research performed at Princeton University and Case Western Reserve University were respectively supported by the Division of Basic Energy Sciences of the U. S. Department of Energy under Contract No. DE-FG02-89ER13988, and by the U. S. Air Force Office of Scientific Research under Grant No. 85-0340.

References

1. Liñán, A. : Acta Astronautica 1, 1007 (1974).
2. Tien, J. S. : Combust. Flame 65, 31 (1986).
3. Sibulkin, M. : Prog. Energy Combust. Sci. 14, 195 (1988).
4. Sohrab, S. H., Liñán, A. and Williams, F. A. : Combust. Sci. Tech. 27, 143 (1982).
5. Law, C. K. : Prog. Energy Combust. Sci. 8, 171 (1982).
6. Abu-Romia, M. M. and Tien, C. L. : Trans. ASME 89, Ser. C : J. Heat Transfer, 321 (1967).

APPENDIX

Broadening of Radiative Diffusion Flames

With the flame sheet located at $\tilde{r}_f$ and having a temperature $\tilde{T}_f$, the temperature and fuel distributions can be solved. Since both the fuel and oxidizer have to be totally consumed at the flame sheet, we obtain from Eq. (2.4) $\tilde{r}_f = \tilde{m} / \ln(1 + \tilde{Y}_{O,\infty})$. Evaluating the temperature at the flame sheet yields

$$\tilde{T}_f = \tilde{T}_s - \tilde{q}_v + \tilde{q}_v \exp\{ \tilde{m} [1 - (1 / \tilde{r}_f)] \} \quad . \tag{A.1}$$

The jump relations can be obtained by integrating Eqs. (2.1) and (2.2) once across the flame sheet, yielding

$$\tilde{r}_f^{\,2} [(d\tilde{T}^+ / d\tilde{r}) - (d\tilde{T}^- / d\tilde{r})]_{\tilde{r}_f} = - I_1 + I_2 \quad , \qquad \tilde{r}_f^{\,2} (d\tilde{Y}_F^- / d\tilde{r})_{\tilde{r}_f} = - I_1 \quad , \tag{A.2}$$

where the superscripts - and + respectively denote the fuel and oxidizer side, and

$$I_1 = (Da / \tilde{T}_f^{\,2}) \int_{\tilde{r}_f^-}^{\tilde{r}_f^+} \tilde{r}^{\,2} \tilde{\rho}^{\,2} \tilde{Y}_F \tilde{Y}_O \exp(- \tilde{T}_{a,K} / \tilde{T}) \, d\tilde{r} \quad , \quad I_2 = Ra \int_{\tilde{r}_f^-}^{\tilde{r}_f^+} \tilde{r}^{\,2} \exp(- \tilde{T}_{a,R} / \tilde{T}) \, d\tilde{r} \quad .$$

Substituting the solutions of $\tilde{T}^{\pm}$ and $\tilde{Y}_F$ into Eq. (2.6) gives

$$\tilde{m} \{ \tilde{T}_\infty + \tilde{Y}_{O,\infty} - \tilde{T}_s + \tilde{q}_v [1 - \exp(\tilde{m})] \} = \tilde{Y}_{O,\infty} I_2 \tag{A.3}$$

and $I_1 = \tilde{m}$. It is seen that there are three unknowns, $\tilde{m}$, $\tilde{T}_F$ and I_2, which need to be determined from the two relations of Eqs. (A.1) and (A. 3). The problem is therefore not closed.

Figure Captions

Figure 1. Variation of the flame temperature $\tilde{T}_f$ and the mass burning rate $\tilde{m}_0$ with the radiative heat loss parameter $\tilde{Ra}^*$. The inset is a schematic defining the problem analyzed.

Figure 2. The extent of flame temperature reduction or reactant leakage as a function of $\tilde{Da}^*$ for fixed values of $\tilde{Ra}^*$.

Figure 3. The extent of flame temperature reduction or reactant leakage as a function of $\tilde{Da}^*$ for fixed values of Γ.

Figure 4. Extinction Damköhler number $\tilde{Da}_E^*$ and flame temperature $\tilde{T}_{f,E}$ as functions of the radiation heat loss parameter Γ.

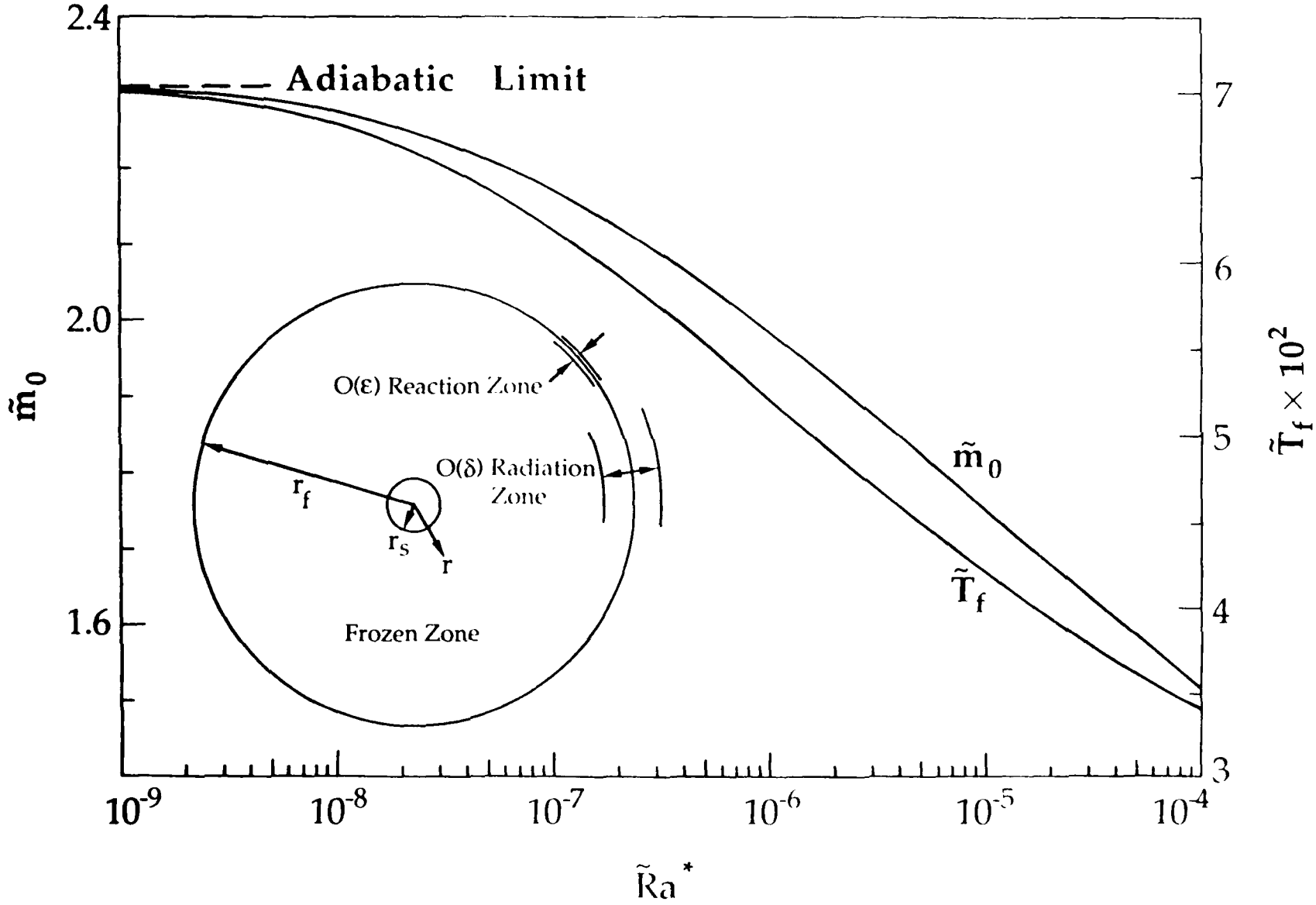
Adiabatic Limit
$\tilde{m}_0$
$\tilde{T}_f \times 10^2$
$\tilde{m}_0$
$\tilde{T}_f$
2.4
2.0
1.6
7
6
5
4
3
10^{-9}
10^{-8}
10^{-7}
10^{-6}
10^{-5}
10^{-4}
$\tilde{Ra}^*$
O(ε) Reaction Zone
O(δ) Radiation Zone
r_f
r_s
r
Frozen Zone

Figure 1

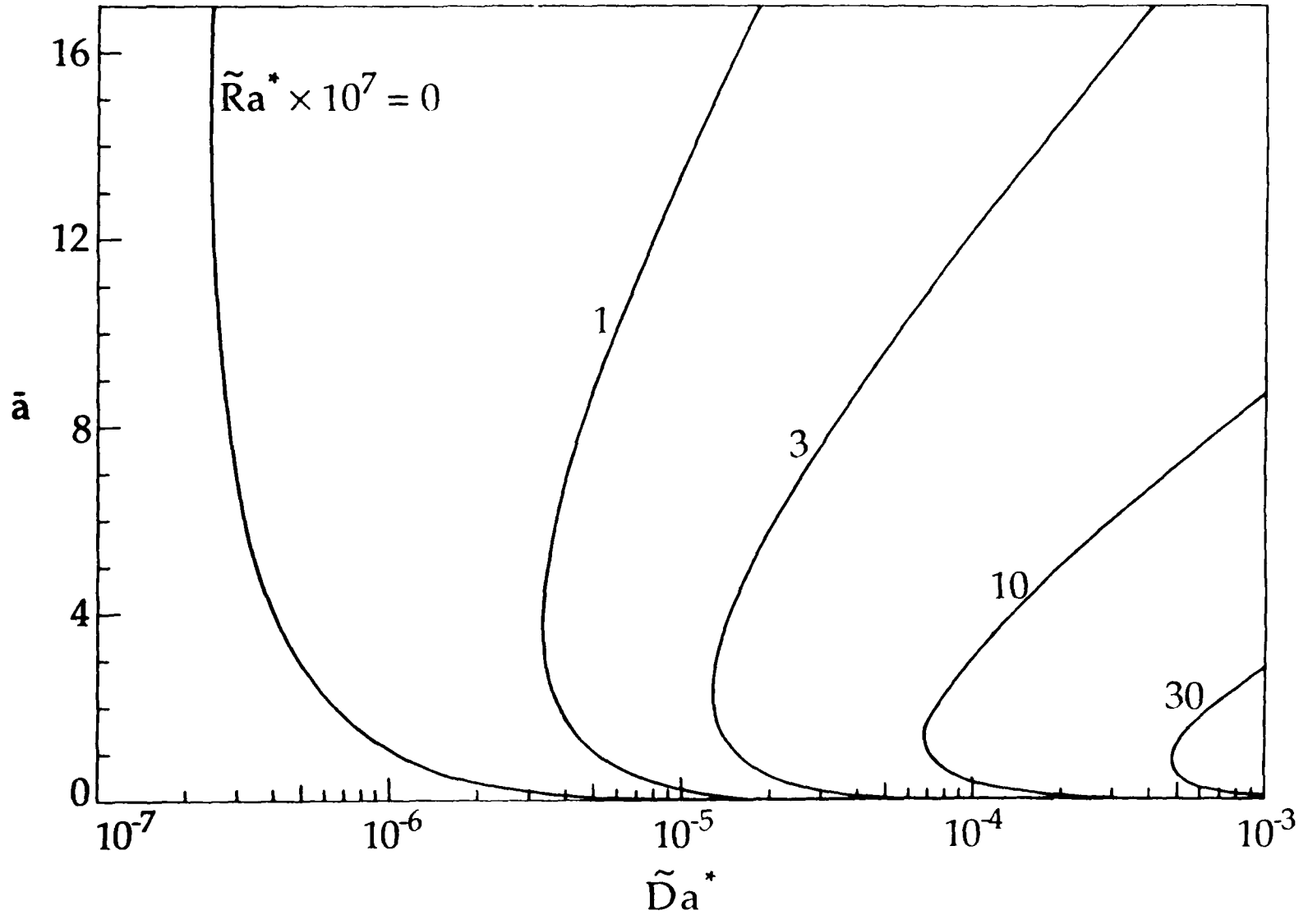
16
12
8
4
0
ā
$\tilde{R}a^* \times 10^7 = 0$
1
3
10
30
10^{-7}
10^{-6}
10^{-5}
10^{-4}
10^{-3}
$\tilde{D}a^*$

Figure 2

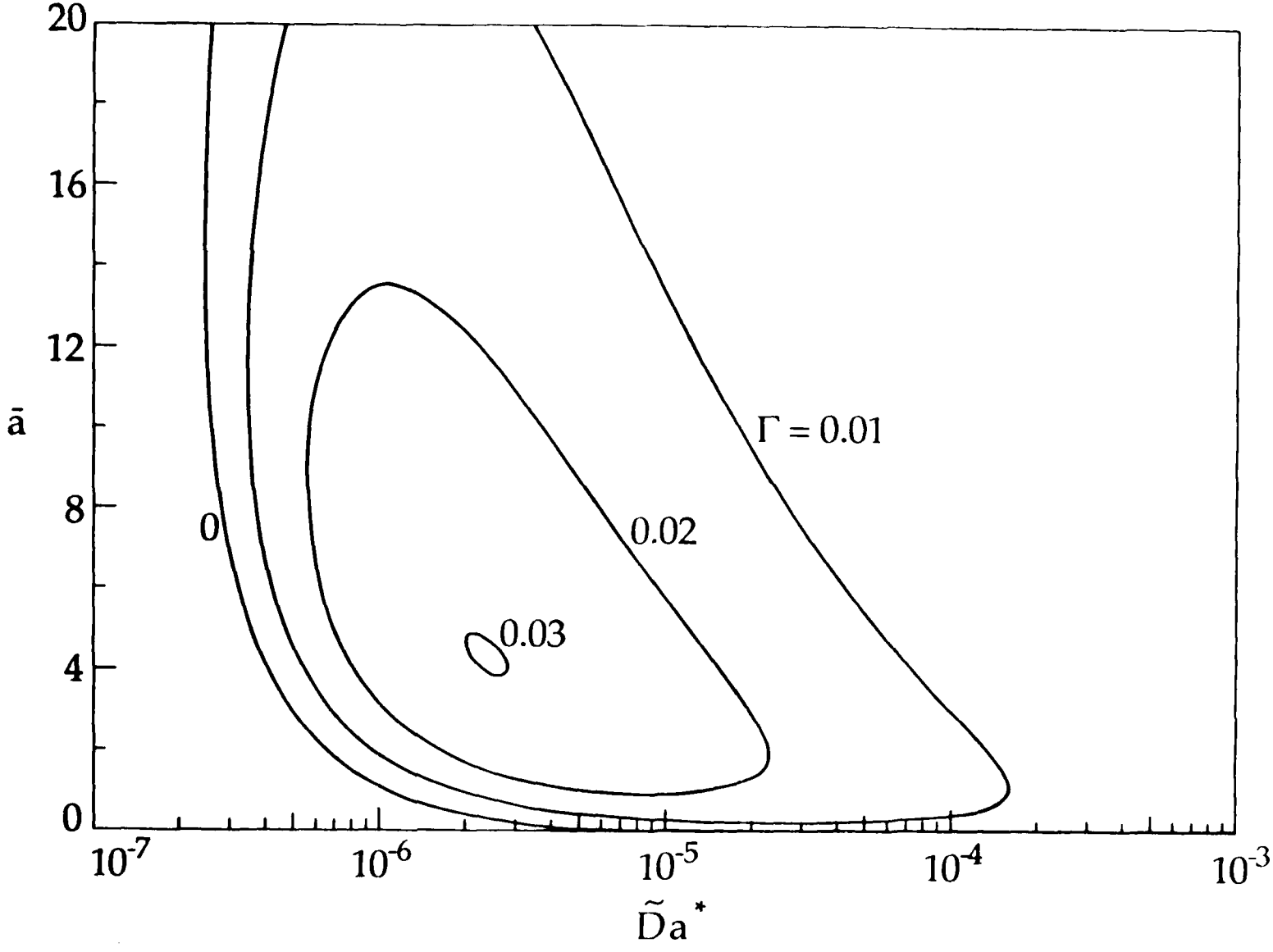

Figure 3

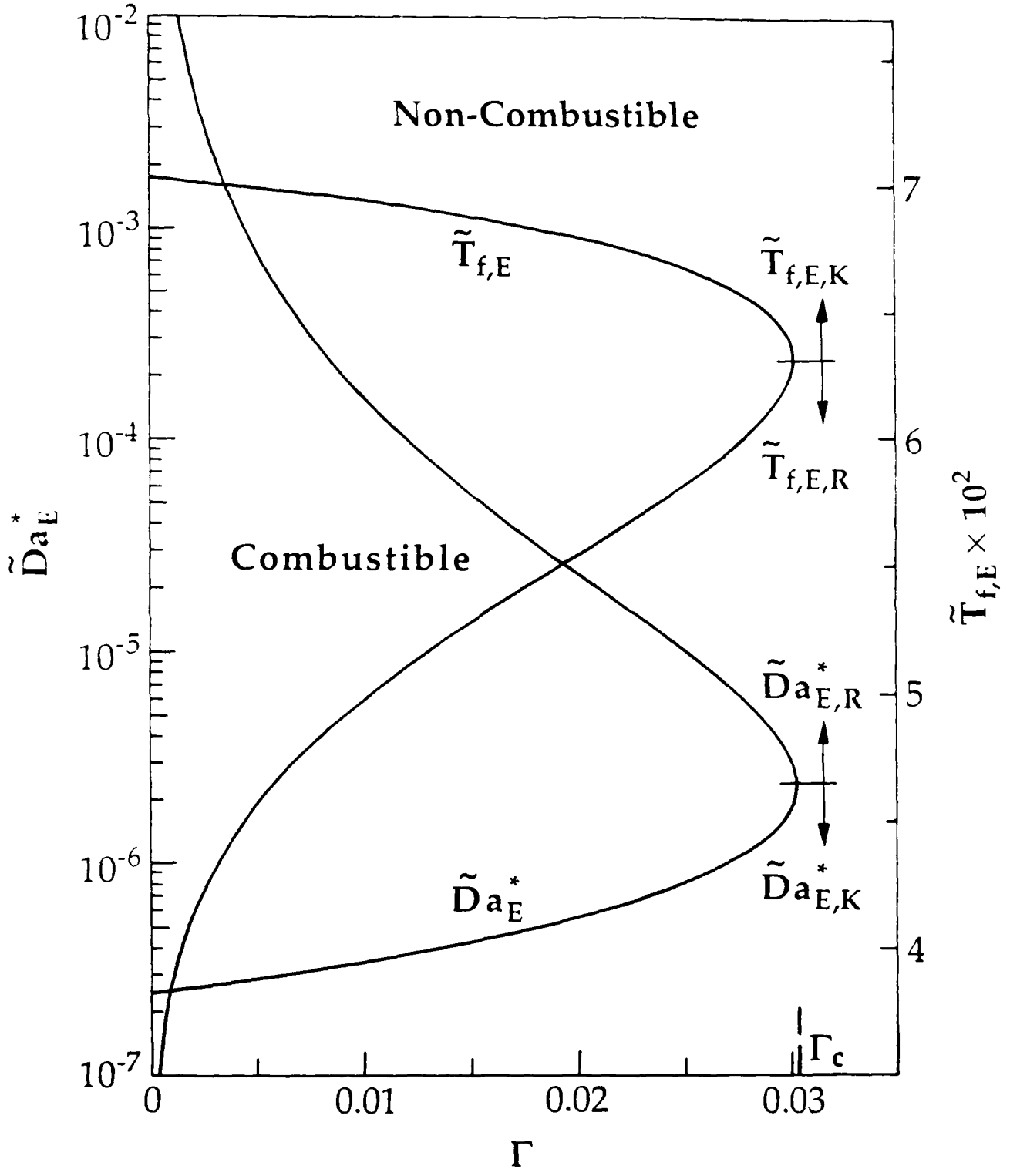
Non-Combustible
Combustible
$\tilde{T}_{f,E}$
$\tilde{T}_{f,E,K}$
$\tilde{T}_{f,E,R}$
$\tilde{Da}^*_E$
$\tilde{Da}^*_{E,R}$
$\tilde{Da}^*_{E,K}$
Γ_c
10^{-2}
10^{-3}
10^{-4}
10^{-5}
10^{-6}
10^{-7}
0
0.01
0.02
0.03
Γ
7
6
5
4
$\tilde{T}_{f,E} \times 10^2$

Figure 4

Appendix C

Submitted to International Journal of Heat and Mass Transfer

DIFFUSION LAYER STRUCTURE IN A THERMOPHORETICALLY AFFECTED FLOW OVER A HOT SURFACE

by

Noureddine Ait Messaoudene and James S. T'ien

Department of Mechanical and Aerospace Engineering

Case Western Reserve University

Cleveland, Ohio 44106

U. S. A.

Abstract

A theoretical analysis is performed to study the distribution of small-size particles in a flow adjacent to a hot wall. Because of the thermophoretic motion, a particle stagnation point is created in the interior of the flow which can produce singularity when particle diffusion is neglected. By including Brownian diffusion and using matched asymptotic expansions, the structure of the inner diffusion layer near the particle stagnation point is resolved. The presented results illustrate how the diffusion layer is evolved and its structural variation with a number of parameters.

I. Introduction

Thermophoresis is the motion of small particles relative to their containing gas induced by a temperature gradient [1, 2]. Because of the existence of thermophoretic velocity, particle concentration distribution can have unusual characteristics which requires special analysis. In the presence of a cold wall, the thermophoretic motion drives the particles toward the wall which affects their deposition rate. In most theoretical works concerning deposition rates, e.g., Refs. [3-7], particle diffusion is neglected. This is because the diffusion coefficient is very small which, in the case of a cold wall, will have only negligible influence on the particle convective flux toward the wall. The neglect of particle diffusion, however, lowers the order of the differential equation of the particle concentration equation. Therefore, the concentration structure in the thin layer next to the wall cannot be studied. Walker, Homsy, and Geyling [8] included Brownian diffusion in their analysis of thermophoretic deposition in flows inside a cold tube. The structure equation is solved using matched asymptotic expansions. They found, however, that because near the wall the fluid velocity is negligible while the thermophoretic velocity is finite, the wall particle deposition rate is unaffected by the diffusion layer.

For a hot wall, the thermophoretic motion drives the particles away from the wall. When particle diffusion is neglected, a particle stagnation point (or surface) is created and a dust-free layer adjacent to the surface is predicted [3, 7, 9, 11]. For low Mach number flow, Goren [3] is the first to show that when the product of thermophoretic coefficient (K) and Prandtl number (Pr) is less than unity, the particle concentration drops to zero quickly at the particle stagnation surface. But when KPr is greater than unity, a singularity occurs - the particle concentration becomes unbounded at the particle stagnation surface. Since in both cases, the concentration gradients become very steep, particle diffusion can become important even when the diffusion coefficient is small. For the case KPr < 1, analysis [11] has been performed for incompressible flow (small temperature difference and low Mach number) including diffusion to assess the degree of particle leakage across the particle stagnation surface. But for KPr > 1, the more severe case for the solution misbehavior (singularity), no remedy has been given.

In this work, a theoretical analysis is given for the particle concentration distribution in a low Mach number, compressible flow over a hot wall. Particle diffusion is included. By using the particle Schmidt number as the large parameter, an inner-outer expansion technique is employed to study the particle diffusion layer structure for both the cases

of KPr greater than unity and less than unity.

II. Governing Equations

The flow to be analyzed is the axisymmetric stagnation-point region of a heated plate as shown schematically in Fig. 1. Experimentally, this configuration can be created either by impinging a jet perpendicularly onto a plate or by placing a blunt body in a windtunnel. The small particles are seeded in the upstream. Fig. 1 shows the existence of two stagnation points: a gas flow stagnation point on the plate surface at $x = y = 0$ and a particle stagnation point at $x = 0$ and $y = y^{*}$ ($\eta = \eta^{*}$). The presence of the particle stagnation point in the interior of the flow field is a result of the particle thermophoretic motion away from the heated plate. To analyze the structure of particle concentration around this particle stagnation point is the objective of this work.

The equations governing the low speed flow (Mach number square much less than unity) in the axisymmetric stagnation-point region are given by the compressible boundary layer equations:

$$\frac{\partial \rho u x}{\partial x} + \frac{\partial \rho v x}{\partial y} = 0 \tag{1}$$

$$\rho\left(u\frac{\partial u}{\partial x} + v\frac{\partial u}{\partial y}\right) = -\frac{\partial p}{\partial x} + \frac{\partial}{\partial y}\left(\mu\frac{\partial u}{\partial y}\right) \tag{2}$$

$$\rho u C_p \frac{\partial T}{\partial x} + \rho v C_p \frac{\partial T}{\partial y} - \frac{\partial}{\partial y}\left(\lambda \frac{\partial T}{\partial y}\right) = 0 \qquad (3)$$

$$\frac{1}{x}\frac{\partial}{\partial x} x \rho u Y + \frac{\partial}{\partial y} \rho v_p Y = \frac{\partial}{\partial y}\left(\rho D \frac{\partial Y}{\partial y}\right) \qquad (4)$$

where Eqs. (1) - (3) are the conventional continuity, momentum and energy equations respectively. The pressure gradient term in Eq. (2) is equal to $-\rho_e u_e \partial u_e/\partial x$ and the x-component free-stream velocity is given by

$$u_e = ax \qquad (5)$$

where a, the velocity gradient, is the parameter characterizing the flow. Eq. (4) is the mass conservation equation for the particles. In Eq. (4), Y is the mass fraction of particles, v_p is the particle velocity which is the sum of gas velocity (v) and thermophoretic velocity (V_t):

$$v_p = v + V_t \qquad (6)$$

The expression for the thermophoretic velocity is:

$$v_t = -K(\mu/\rho)\nabla T/T \qquad (7)$$

where K is the thermophoretic coefficient whose magnitude depends on the regime of the flow [12]. The value of K normally taken is between 0.2 and 1.25 and in the present study

it is treated as a parameter.[1] The last term in Eq. (4) represents particle (Brownian) diffusion and D is the diffusion coefficient which is normally very small.

The boundary conditions for the flow and the temperature fields are:

$$y = 0: \quad u = v = 0 \quad , \quad T = T_w \tag{8}$$

$$y \to \infty : \quad u = u_e \quad , \quad T = T_\infty \tag{9}$$

and for the particles:

$$y = 0: \quad Y = 0 \tag{10}$$

$$y \to \infty: \quad Y = Y_\infty \tag{11}$$

The condition of $Y = 0$ in Eq. (10) is the result of assuming that we have a "sticky" wall that will act as a perfect sink for the particles [15]. The condition of $Y = Y_\infty$ in Eq. (11) indicates that the particles are seeded in the free stream. To proceed further, the following assumptions are added:

1. the gas obeys ideal gas law and the product $\rho\mu$ is a constant,

[1]Experimental determination of K is a difficult task [13]. A novel measurement technique using counterflow diffusion flames has recently been suggested [14].

2. gas heat capacity C_p, the thermophoretic coefficient K, and the Prandtl number Pr are constant,

3. the mass fraction of particles is much smaller than unity which does not affect the overall continuity equation,

4. the Schmidt number (based on Brownian particle diffusion coefficient) is constant,

5. the particles are of uniform size and inert. There is no particle chemical reaction, nucleation, condensation, coagulation or break-up.

Next, the Howarth-Dorodnitsyn transformation for compressible boundary layer is introduced:

$$\eta = \sqrt{\frac{a}{\rho_e \mu_e}} \int_0^y \rho dy \quad \text{and} \quad s = \frac{a}{4}\rho_e \mu_e x^4 \tag{12}$$

$$u = u_e \frac{f'}{2} \quad \text{and} \quad v = -\frac{1}{\rho}\sqrt{\rho_e \mu_e a}\, f \tag{13}$$

where s and η are the transformed x and y coordinates and f is a modified streamfunction. Using Eqs. (12, 13) and introducing nondimensional temperature θ ($= T/T_\infty$), Eqs. (1-3) become:

$$f''' + ff'' = \frac{1}{2}\left[f'^2 - 4\theta\right] \tag{15}$$

$$\frac{1}{Pr}\theta'' + f\theta' = 0 \tag{16}$$

where superscript ´ denotes d/dη.

The boundary conditions [Eqs. (8-9)] give

$$\eta = 0: \quad \theta = \theta_w \quad f = f' = 0$$
$$\eta \to \infty: \quad \theta = 1 \quad f' = 2 \tag{17}$$

For the particles, Eq. (4), with Eqs. (6-7), is transformed into:

$$\frac{1}{Sc}Y'' + V(\eta)Y' + F(\eta)Y = 0 \tag{18}$$

where

$$V(\eta) = f + K\theta'/\theta \tag{19}$$

$$F(\eta) = K(\theta\theta'' - \theta'^2)/\theta^2 \tag{20}$$

Equations (15-17) can be solved first. The velocity and temperature fields obtained can then be used in Eq. (18) for the solution of particle mass fraction. The decoupling of particle distribution from the flow field computation is the result of assumption of dilute particle concentration. We will now concentrate on developing the analytic solution for Eq. (18) subject to boundary conditions (10-11). For particle size ranging from 10 nm to a micron, the Schmidt number is typically high and will range from 10^2 to 10^6 [13]. Therefore, 1/Sc can

be regarded as a small parameter in Eq. (18). The quantity V in Eq. (18) represents the particle velocity. As shown in Eq. (19), V consists of a gas flow component f and a thermophoretic component $K\theta'/\theta$. In this problem, f starts with zero value at $\eta = 0$, increases monotonically as η increases and θ' is negative at $\eta = 0$, increases with η and reaches zero at large η. Thus at some location above the heated plate, denoted by η^*, V is equal to zero. This is the particle stagnation point. As shown schematically in Fig. 1, on one side of η^*, V is positive and on the other side, it is negative, i.e., V changes sign at η^*. Using 1/Sc as the small expansion parameter, Eq. (18) constitutes a singularly perturbed differential equation with a *turning point* [16-19].

III. Analysis

The analytic solution for Eq. (18) with boundary conditions (10-11) will be presented in this section using the matched-asymptotic expansion technique [20-21].Equation (18) gives rise to two regions using the perturbation method: an outer region where only convection (including thermophoresis) is important, and an inner region near η^* where diffusion is also important.

Outer region:

Diffusion is negligible and Eq. (18) becomes

$$V(\eta)Y' + F(\eta)Y = 0 \tag{21}$$

Applying the boundary conditions, the solutions are:

$$0 < \eta < \eta^{\bullet} \quad , \quad Y = 0 \tag{22}$$

$$\eta > \eta^{\bullet} \quad , \quad \frac{Y}{Y_{\infty}} = \exp\int_{\eta}^{\infty} \frac{F(\eta)}{V(\eta)}d\eta \tag{23}$$

In $\eta > \eta^{\bullet}$, $V(\eta) > 0$, Eq. (23) shows that if $F(\eta^{\bullet}) < 0$, $Y(\eta^{\bullet}) \rightarrow 0$ which matches the value from Eq. (22) although the gradients $dY/d\eta$ are not continuous at $\eta^{\bullet}$. If, however, $F(\eta^{\bullet}) > 0$, Eq. (23) indicates $Y(\eta^{\bullet})/Y_{\infty}$ becomes unbounded. Appendix A shows that the sign of $F(\eta^{\bullet})$ depends on the value of the product of Prandtl number and thermophoretic coefficient: $F(\eta^{\bullet}) \gtreqless 0$ if $KPr \gtreqless 1$. When $KPr > 1$, the other solution is singular at the particle stagnation point. This singularity can be removed in the inner solution where particle diffusion is included.

Inner region

In order to simplify the analytical treatment we first consider a region of thickness $2\Delta\eta$ around $\eta^{\bullet}$ in which $V(\eta)$ and $F(\eta)$ can be linearized. Eq. (18) can be rewritten as:

$$\frac{1}{Sc}Y'' + (\eta - \eta^{\bullet})V'(\eta^{\bullet})Y' + \left[F(\eta^{\bullet}) + (\eta - \eta^{\bullet})F'(\eta^{\bullet})\right]Y = 0 \tag{24}$$

upon changing the variables to

$$\xi = \frac{\eta^{\bullet} - \eta}{\Delta\eta}$$

this becomes

$$\varepsilon \frac{d^2Y}{d\xi^2} + \xi \frac{dY}{d\xi} + (A + B\xi)Y = 0 \qquad (25)$$

with boundary conditions

$$Y(-1) = 0 \; ; \; Y(+1) = Y_{+1}$$

where

$$\varepsilon = 1/\left[Sc\Delta\eta^2 V'(\eta^{\bullet})\right]$$

$$A = F(\eta^{\bullet})/V'(\eta^{\bullet})$$

$$B = \Delta\eta F'(\eta^{\bullet})/V'(\eta^{\bullet}) \qquad (26)$$

$$Y_{+1} = Y_{\infty} \exp\left[\int_{\eta^{\bullet}+\Delta\eta}^{\infty} \frac{F(\eta)}{V(\eta)}\, d(\eta)\right]$$

and $\xi = 0$ corresponds to $\eta = \eta^{\bullet}$. Near $\eta^{\bullet}$, $V(\eta) \simeq 0$ and the first term in Eq. (25) can only be balanced by the last term so that an inner layer of thickness $\delta \sim O(\sqrt{\varepsilon})$ will exist. Outside this inner layer and in $-1 < \xi < +1$ a linearized outer solution will be given by

$$Y = 0 \quad \text{for } -1 \leq \xi < 0$$

$$Y = Y_{+1}\xi^{-A}\exp\left[-B\left(\xi-1\right)\right] \quad \text{for } 0 < \xi < +1 \tag{27}$$

which can be rewritten in terms of η:

$$Y = G\left(\eta-\eta^{*}\right)^{-A}\exp\left[-\frac{F'(\eta^{*})}{V'(\eta^{*})}\left(\eta-\eta^{*}\right)\right] \tag{28}$$

where

$$G = Y_{+1}\Delta\eta^{A}e^{B}$$

and it can be shown that G is independent of the choice of $\Delta\eta$ within the neighborhood of η^{*} [21]. Note that we must have $\Delta\eta \gtrsim \delta$, so that from the definition of ε in Eq. (26) we get

$$\delta \sim O\left[\frac{1}{\left(ScV'(\eta^{*})\right)^{.25}}\right]$$

Now we introduce a stretched variable, $\nu = \xi/\sqrt{\varepsilon}$, to transform Eq. (25) into

$$\frac{d^2Y}{d\nu^2} + \nu\frac{dY}{d\nu} + \left(AY + \sqrt{\varepsilon}\,B\right)Y = 0 \tag{29}$$

since ε is a small parameter Eq. (29) can be approximated by

$$\frac{d^2Y}{d\nu^2} + \nu\frac{dY}{d\nu} + AY = 0 \tag{30}$$

The general solution to Eq. (30) is

$$Y = e^{-\nu^2/4}\left[C_1 D_{A-1}(\nu) + C_2 D_{-A}(i\nu)\right] \tag{31}$$

where the D_n's are parabolic cylinder functions [23] and C_1, C_2 constants of integration.

Using the matching principle described in [20, 21] the asymptotic expansions of the D_n's [23] and the boundary conditions, the following composite expansions are obtained:

$$-1 \le \xi \le 0 \quad (\eta < \eta^*)$$

$$Y_-(\xi) = Y_{+1}\exp(B)(\sqrt{\varepsilon})^{-A}\exp(-\xi^2/4\varepsilon)$$

$$\left[\frac{\Gamma(1-A)}{\sqrt{2\pi}}\exp\left[\left(1-A\right)\pi i\right]D_{A-1}\left(\xi/\sqrt{\varepsilon}\right) + i^A D_{-A}\left(i\xi/\sqrt{\varepsilon}\right)\right] \tag{32a}$$

$$0 \le \xi \le 1 \quad (\eta > \eta^*),$$

$$Y_+(\xi) = Y_{+1}\exp(B)(\sqrt{\varepsilon})^{-A}\exp(-\xi^2/4\varepsilon)\left[\frac{\Gamma(1-A)}{\sqrt{2\pi}}\exp\left[\left(1-A\right)\pi i\right]D_{A-1}\left(\xi/\sqrt{\varepsilon}\right)\right.$$

$$\left. + i^A D_{-A}\left(i\xi/\sqrt{\varepsilon}\right)\right] + Y_{+1}\exp(B)(\xi)^{-A}\left[\exp(-B\xi)-1\right] \tag{32b}$$

and using the fact that

$$D_{-n}(iZ) = \frac{\Gamma(1-n)}{\sqrt{2\pi}} \left[\exp(n\pi i/2) D_{n-1}(Z) + \exp\left(\frac{-n\pi i}{2}\right) D_{n-1}(-Z)\right] \quad (33)$$

we obtain:

$$Y_-(\xi) = Y_{+1}\exp(B)(\sqrt{\varepsilon})^{-A} \frac{\Gamma(1-A)}{\sqrt{2\pi}} \exp(-\xi^2/4\varepsilon) D_{A-1}(-\xi/\sqrt{\varepsilon}) \quad (34)$$

and

$$Y_+(\xi) = Y_-(\xi) + Y_{+1}\exp(B)(\xi)^{-A}\left[\exp(-B\xi) - 1\right] \quad (35)$$

this can be rewritten in terms of η:

$$Y_-(\eta) = G\left[ScV'(\eta^*)\right]^{A/2} \frac{\Gamma(1-A)}{\sqrt{2\pi}} \exp\left[-ScV'(\eta^*) \frac{(\eta-\eta^*)^2}{4}\right]$$

$$D_{A-1}\left[-\sqrt{ScV'(\eta^*)}\ (\eta-\eta^*)\right] \quad (36)$$

$$Y_+(\eta) = Y_-(\eta) + G(\eta-\eta^*)^{-A}\left\{\exp\left[-\frac{F'(\eta^*)}{V'(\eta^*)}\left(\eta-\eta^*\right)\right]-1\right\} \quad (37)$$

Eqs. (36-37) give the particle mass fraction profile in the diffusional inner layer near the stagnation point. Together with the outer solution, Eqs. (22-23), they give the

complete distribution of particle mass fraction in the flow field. To see that the singularity at the particle stagnation point is removed, we get from Eq. (36) or (37):

$$Y(\eta^*) = G\left[2ScV'(\eta^*)\right]^{A/2} \frac{\Gamma(1-A)}{2\Gamma(1-A/2)}$$

From the above expression, we see that $Y(\eta^*)$ will grow as $\left(\sqrt{Sc}\right)^A$. For any finite value of Sc, $Y(\eta^*)$ will be bounded. In the physical systems, Sc will be finite and the present analysis is valid for values of Sc up to about 10^6. Beyond this value the inertia of the particles may become important.

IV. Discussion

In this section, selected graphical presentations will be given for the analytical solutions just obtained. This is to illustrate the importance of Brownian diffusion near the particle stagnation point especially when the product of thermophoretic coefficient and Prandtl number is greater than unity.

Fig. 2 shows the particle mass fraction profiles near the stagnation point (η^*) as given by Eqs. (36) and (37) for Sc = 10^5, Pr = 1 and KPr = .6 and 1.5. Also shown in the dashed lines are the solutions with diffusion neglected. For KPr < 1, we see that particle diffusion modifies the concentration

profile--there is a leakage through the stagnation point and the concentration gradient drops smoothly toward zero. This is similar to finding in Ref. 11. More drastic is the case for KPr > 1 (= 1.5). The dashed curved in the bottom half of Fig. 2 shows that without considering diffusion, the mass fraction becomes unbounded at the stagnation point. When diffusion is included, however, a peak of Y/Y_∞ occurs slightly upstream of the stagnation point η^*, the particle concentration then drops steeply, passing through η^*, to zero. Thus, we see that particle Brownian diffusion, although having a very small diffusion coefficient, produces drastically different concentration profiles when KPr is greater than unity.

Fig. 3 shows the particle profile as a function of η from the wall boundary to the free stream for Pr = 1, K = 1.5 (Pr x K = 1.5) and Sc. = 10^4. In this figure, not only the inner solutions and also the full range of outer solutions are utilized.

In Fig. 4 the particle mass fraction profiles near their stagnation plane are shown for Sc ranging from 10^2 to 10^6 for Pr = 1 and K = 1.5. As Sc increases the peak sharpens, the peak value increases and the peaking location moves closer to η^*.

Fig. 5 shows the particle mass fraction profile for different values of K for Sc = 10^4 and Pr = 1. We see that with the introduction of Brownian diffusion the behavior of the

solution changes monotonically and smoothly as KPr changes from values less than one to more than one. We also see that as K decreases, the particles stagnation plane moves closer to the hot boundary due to the decrease in thermophoretic velocity.

The analytic solution given by the asymptotic expansion has also been compared with direct numerically integrated solutions of Eq. (18). For $Sc = 10^2$ to 10^4 the solutions from the two methods are practically indistinguishable. As expected, the asymptotic solution breaks down for moderate values of the Schmidt number. At $Sc = 10$ the difference between numerical and asymptotic solutions becomes appreciable and in the analytic solution a slope discontinuity at η^* becomes visible due to the limit of validity of the expansions of the D_n's. Direct numerical solution of Eq. (18) for Sc beyond 10^4 becomes increasingly difficult because of the demand of increasingly smaller grid size.

Nomenclature

$A = F(\eta^{\bullet}))/V'(\eta^{\bullet})$

a stagnation-point potential flow velocity gradient

$B = \Delta\eta F'(\eta^{\bullet})/V(\eta^{\bullet})$

F defined in Eq. (20)

G defined in Eq. (28)

f nondimensionalized stream function

K thermophoretic coefficient

Pr Prandtl number

Sc Schmidt number

T absolute temperature

V nondimensional velocity Eq. (19)

Y particle mass fraction, (mass of particle/unit volume)/(total mass of gas and particle/unit volume)

y distance away from the heated wall

Greek Symbols

μ coefficient of dynamic viscosity

ρ density

η similarity variable Eq. (12)

θ T/T_{∞}, nondimensional Temperature

δ concentration inner layer thickness

ξ $(\eta - \eta^{\bullet})\Delta\eta$

ν stretched variable

ε small parameter, see Eq. (26)

Nomenclature (continued)

Subscripts

t	thermophoretic
e	boundary layer edge
∞	free stream conditions
-	$\eta < \eta^{\bullet}$
+	$\eta > \eta^{\bullet}$

Superscripts

•	particle stagnation plane location

Acknowledgement

This research has been supported by the United States Air Force Office of Scientific Research through Grant 85-0340. AMN would also like to acknowledge support from the Ministry of Higher Education of Algeria.

References

1. Friedlander, S. K.: Smoke, Dust and Haze, Wiley, New York (1977).

2. Talbot, L.: Thermophoresis - A Review, in Rarefied Gas Dynamics, Part I (Edited by S. S. Fisher), Prog. Astronaut. Aeronaut, 74, 467-488 (1981).

3. Goren, S.: Thermophoresis of Aerosol Particles in the Laminar Boundary Layer of a Flat Plate, J. of Coll. and Interf. Sci., 61, 77-85 (1977).

4. Batchelor, G. K. and Shen, C.: Thermophoretic Deposition of Particles in Gas Flowing Over Cold Surfaces, J. of Coll. and Interf. Sci., 107, 21-37 (1985).

5. Shen, C.: Thermophoretic Deposition of Particles onto Cold Surfaces of Bodies in Two-Dimensional and Axisymmetric Flows, J. of Coll. and Interf. Sci., Vol. 127, No. 1 (1989).

6. Homsy, G. M., Geyling, F. T., and Walker, K. L.: Blasius Series for Thermophoretic Deposition of Small Particles, J. of Coll. and Interf. Sci., 83, 495-501 (1981).

7. Garg, V. K. and Jayaraj, S.: Thermophoresis of Aerosol Particles in Laminar Flow Over Inclined Plates, Int. J. Heat and Mass Trans., Vol. 31, 875-890 (1988).

8. Walker, K. H., Homsy, G. M., and Geyling, F. T.: Thermophoretic Deposition of Small Particles in Laminar Tube Flow, J. of Coll. and Interf. Sci., 69, 138-147 (1979).

9. Gokoglu, S. A. and Rosner, D. E.: Prediction and Rational Correlation of Thermophoretically Reduced Particle Mass Transfer to Hot Surfaces Across Laminar and Turbulent Forced-Convection Gas Boundary Layers, Chem. Eng. Comm., Vol. 44, pp. 107-120 (1986).

10. Stratman, F., Fissan, H., Papperger, A., and Friedlander, S. K.: Suppression of Particle Deposition to Surfaces by the Thermophoretic Force, Aerosol Sci. Technol. 9, 115-121 (1988).

11. Friedlander, S. K., Fernandez de la Mora, J., and Gokoglu, S. A.: Diffusive Leakage of Small Particles Across the Dust-Free Layer Near a Hot Wall, J. Coll. Interf. Sci., 125, 351-355 (1988).

12. Talbot, L., Chen, R. K., Scheffer, R. W., and Willis, D. R.: Thermophoresis of Particles in a Heated Boundary Layer, J. of Fl. Mech., 101, 737-758 (1980).

13. Flower, W. L.: Measurements of the Diffusion Coefficient for Soot Particles in Flames, Physical Review Letters, 51, 2287-2290 (1983).

14. Gomez, A., Smooke, M. D., and Rosner, D. E.: Application of Counterflow Diffusion Flames to the Determination of Particle Thermophoretic Diffusivities, Eastern States Section Meeting, The Combustion Institute, Gaithersburg, Maryland (1987).

15. Gokoglu, S. A. and Rosner, D. E.: Thermophoretically Augmented Mass Transfer Rates to Solid Walls Across Laminar Boundary Layers, AIAA Journal, 24, 172-179 (1986).

16. O'Malley, R. E.: On Boundary Value Problems for a Singularly Perturbed Differential Equation with a Turning Point, SIAM J. Math. Anal., F, 479-490 (1970).

17. Grassman, J. and Matkowski, B. J.: A Variational Approach to Singularly Perturbed Boundary Value Problems for Ordinary and Partial Differential Equations with Turning Points, Ibid, 32, 588-597 (1977).

18. Kresiss, H. O. and Parter, S. V.: Remarks on Singular Perturbations with Turning Points, Ibid, 5, 230-251 (1974).

19. Pearson, C. E.: On a Differential Equation of Boundary Layer Type, J. of Math and Phys., 47, 134-154 (1968).

20. Nayfeh, A. H.: Perturbation Methods, Wiley Interscience (1973).

21. Van Dyke, M.: Perturbation Methods in Fluid Mechanics, Academic Press (1964).

22. N. Ait Messaoudene: Particle Distribution Near the Stagnation Point Induced by Thermophoretic Motion With and Without Combustion, Ph.D. Thesis, Case Western Reserve University, January, 1989.

23. Abromwitz, M.: Handbook of Mathematical Functions, Vol. 55, p. 686, N. B. S. Appl. Math Series (1964).

Appendix A: Sign of $F(\eta^*)$

From the definition of $F(\eta)$ we have

$$F(\eta^*) = K\left[\frac{\theta\theta'' - \theta'^2}{\theta^2}\right]_{\eta=\eta^*} \tag{A.1}$$

so $F(\eta^*)$ has the same sign as $(\theta\theta'' - \theta'^2)_{\eta=\eta^*}$. Furthermore, the energy equation for θ is

$$\frac{1}{Pr}\theta'' + f\theta' = 0 \tag{A.2}$$

and at η^*, $V(\eta^*) = 0$ therefore $f(\eta^*) = -K\left(\frac{\theta'}{\theta}\right)_{\eta=\eta^*}$ (A.3)

Upon replacing Eq. (A.3) in (A.2) we obtain

$$\theta\theta'' = PrK\theta'^2 \text{ at } \eta=\eta^* \tag{A.4}$$

so that $(\theta\theta'' - \theta'^2)_{\eta=\eta^*} = \theta'^2(\eta^*)[PrK - 1]$ (A.5)

and from Eqs. (A.5) and (A.1) we see that

$$F(\eta^*) \gtrless 0 \quad \text{if } PrK \gtrless 1 \tag{A.6}$$

List of Figures

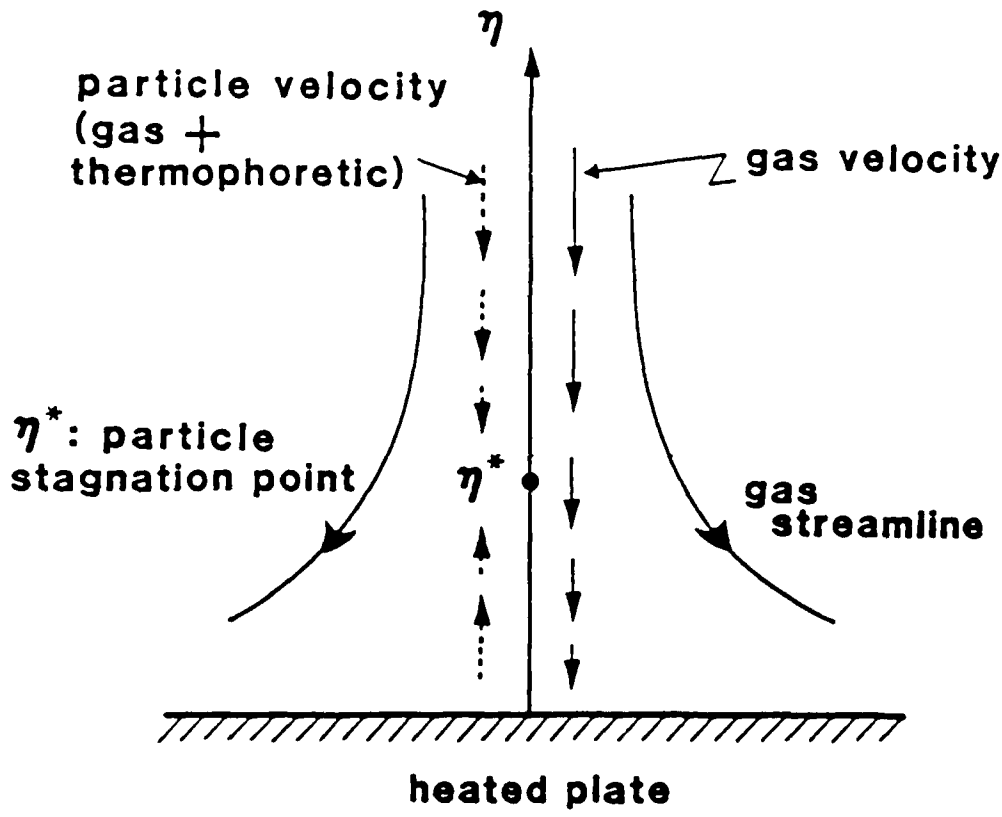
η
particle velocity
(gas +
thermophoretic)
gas velocity
η*: particle
stagnation point
η*
gas
streamline
heated plate

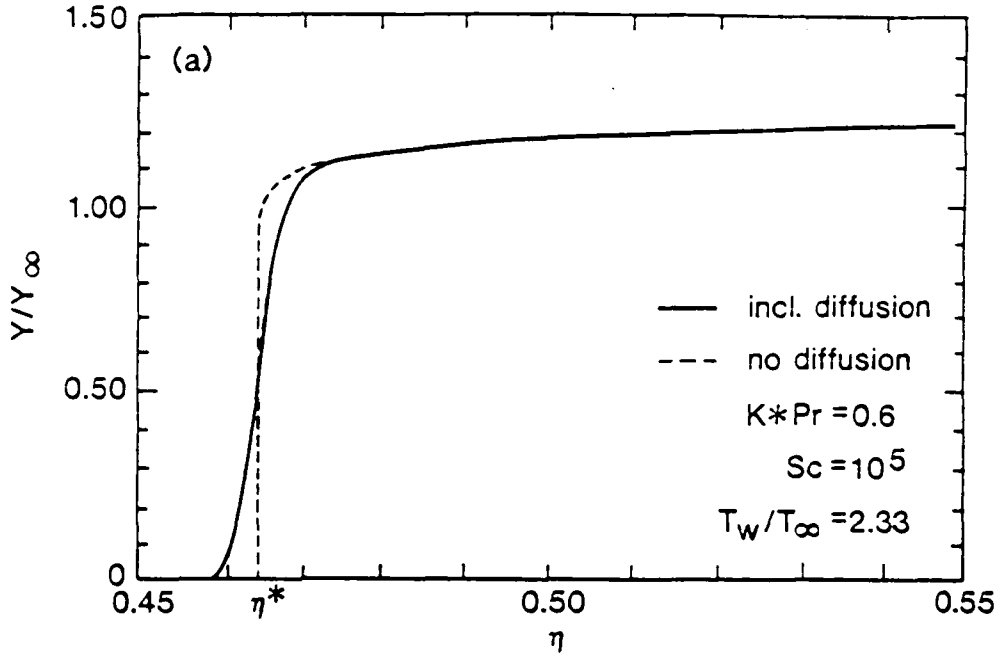
(a)
1.50
1.00
0.50
0
Y/Y∞
0.45
η*
0.50
0.55
η
incl. diffusion
no diffusion
K*Pr =0.6
Sc =10^5
Tw/T∞ =2.33

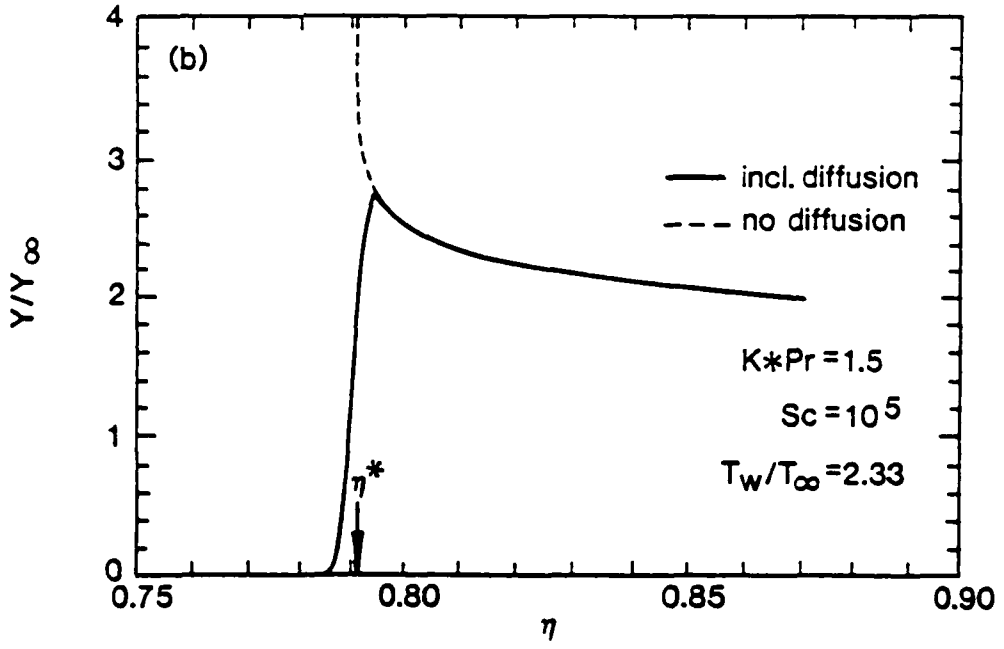
(b)
4
3
2
1
0
Y/Y∞
0.75
0.80
0.85
0.90
η
η*
incl. diffusion
no diffusion
K*Pr =1.5
Sc =10^5
Tw/T∞ =2.33

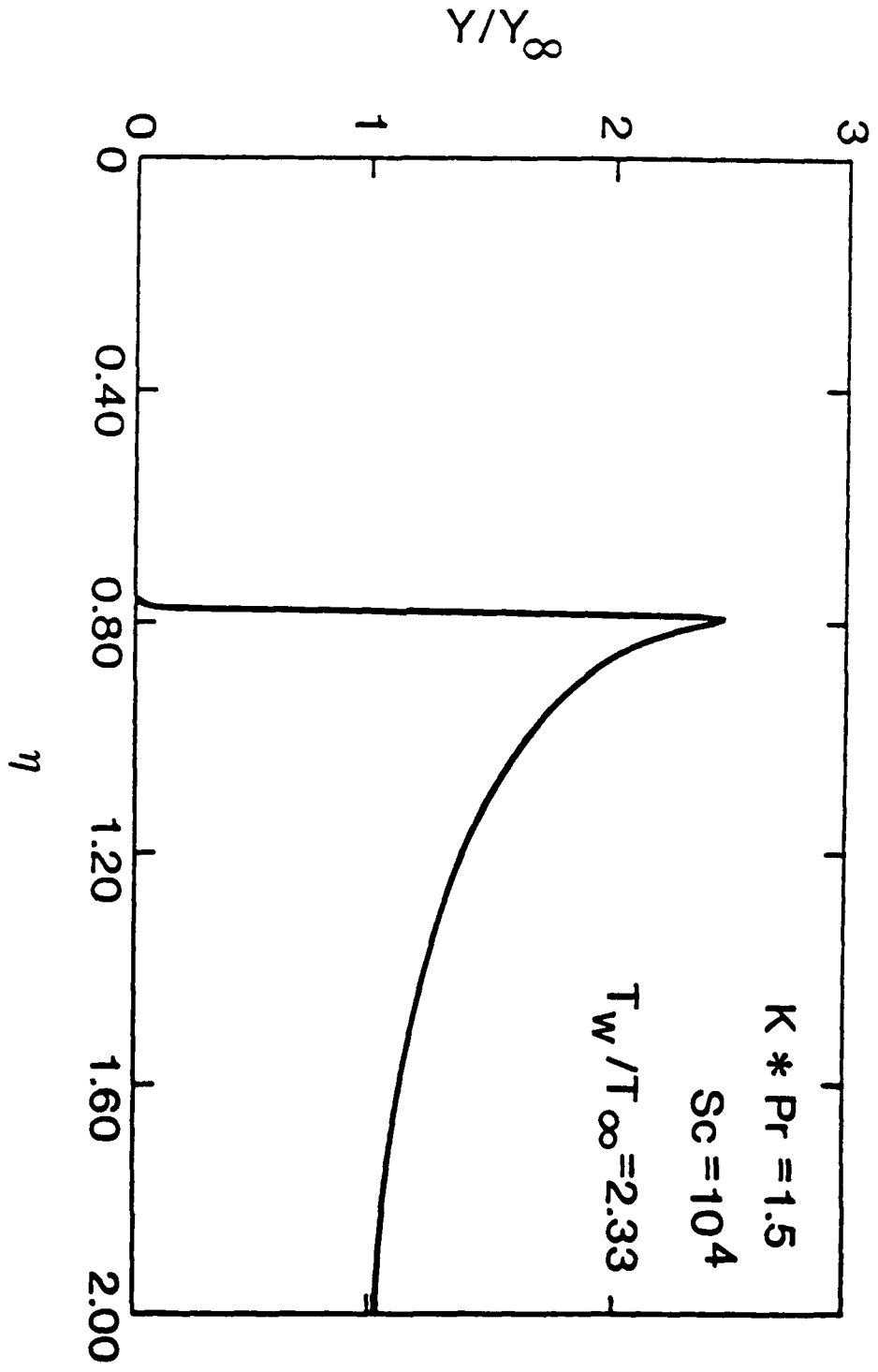
Y/Y_∞
0
1
2
3
0
0.40
0.80
1.20
1.60
2.00
η
K * Pr =1.5
Sc =10^4
T_w/T_∞=2.33

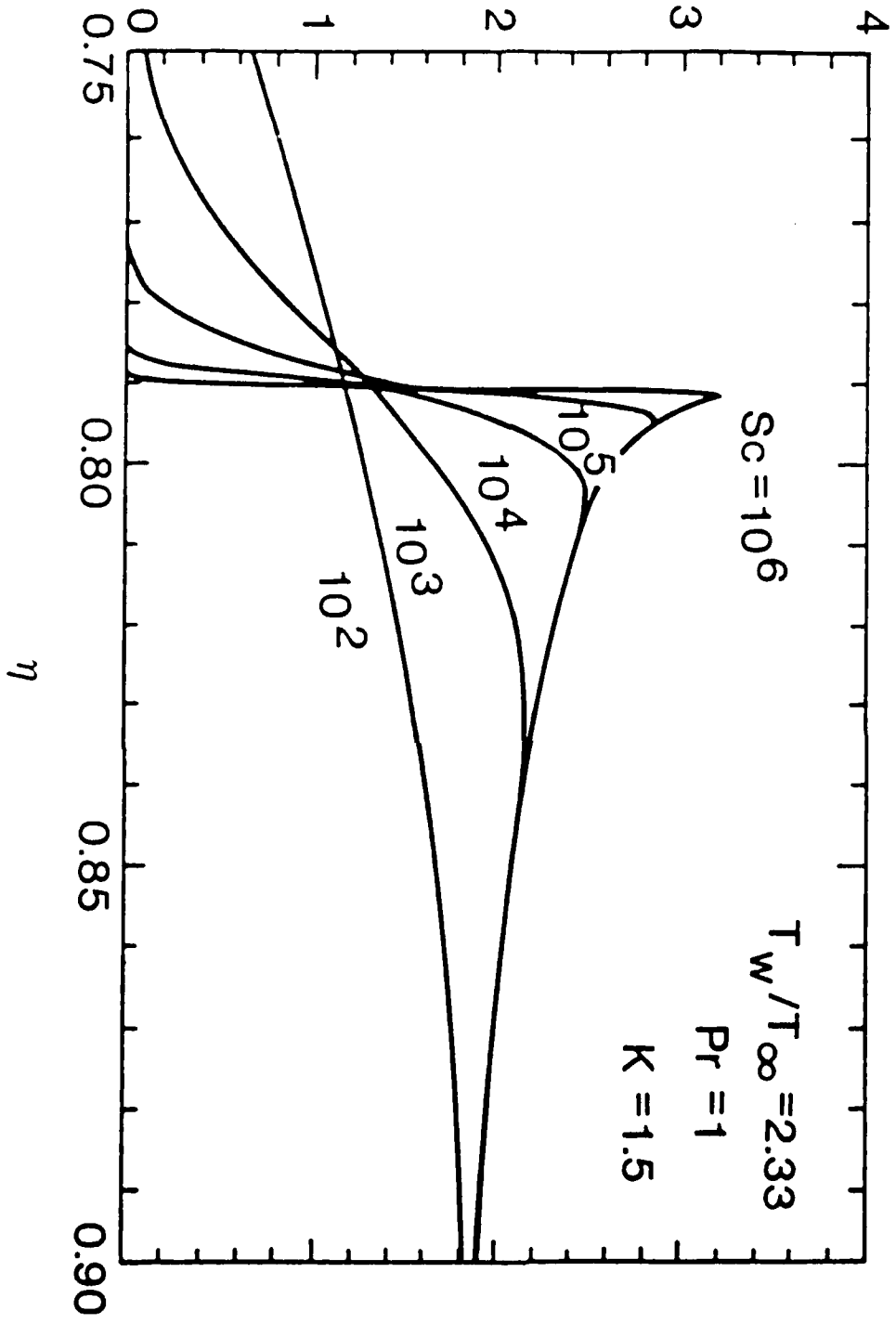
Y/Y8
0
1
2
3
4
0.75
0.80
0.85
0.90
η
Sc=10^6
10^5
10^4
10^3
10^2
Tw/T∞=2.33
Pr=1
K=1.5

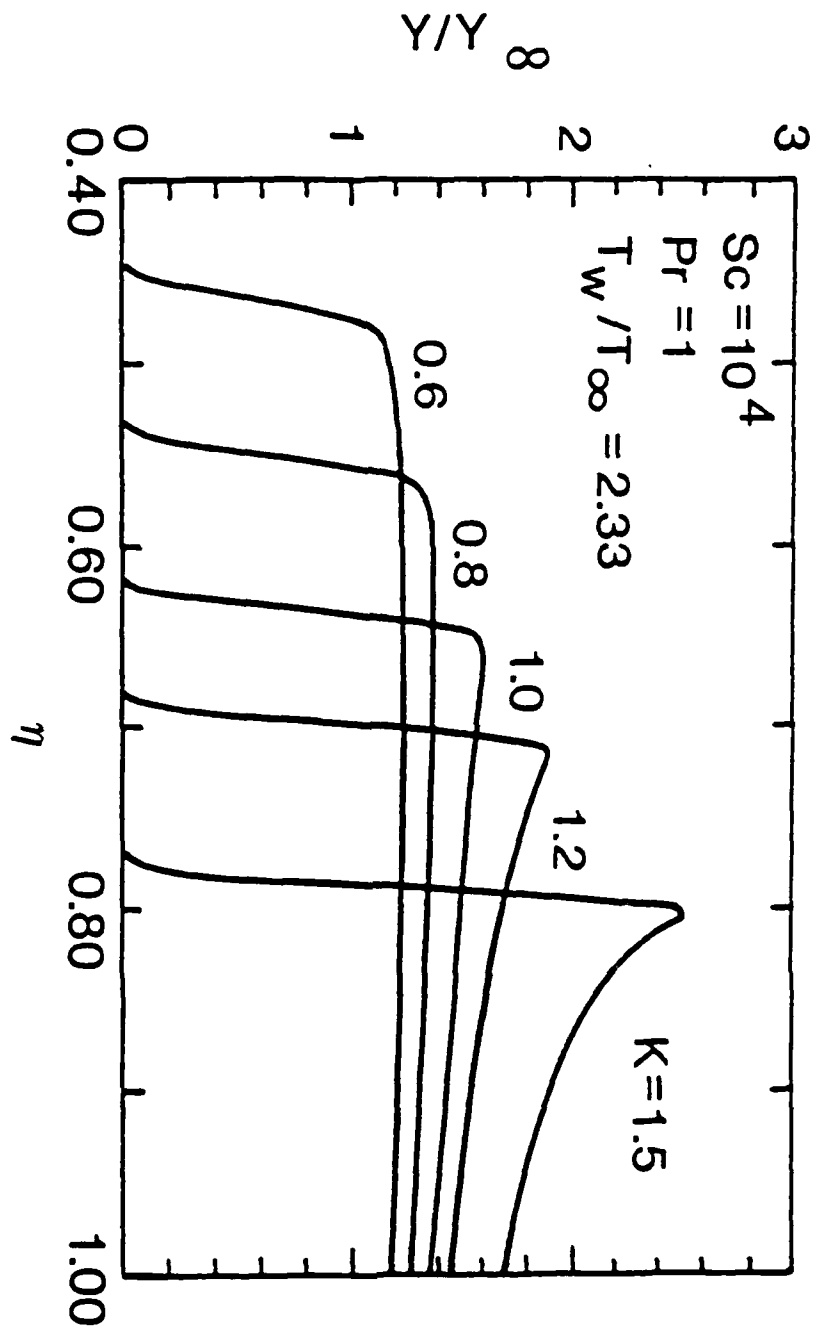
Y/Y δ
0
1
2
3
0.40
0.60
0.80
1.00
η
Sc = 10^4
Pr = 1
T_w/T_∞ = 2.33
0.6
0.8
1.0
1.2
K=1.5